

Stratified Topological Autonomy for Long-Range Coordination (STALC)

Cora A. Dimmig^{1,2}, Adam Goertz¹, Adam Polevoy^{1,2}, Mark Gonzales², Kevin C. Wolfe¹, Bradley Woosley³, John Rogers³, and Joseph Moore^{1,2}

Abstract—Achieving unified multi-robot coordination and motion planning in complex environments is a challenging problem. In this paper, we present a hierarchical approach to long-range coordination, which we call Stratified Topological Autonomy for Long-Range Coordination (STALC). In particular, we look at the problem of minimizing visibility to observers and maximizing safety with a multi-robot team navigating through a hazardous environment. At its core, our approach relies on the notion of a *dynamic topological graph*, where the edge weights vary dynamically based on the locations of the robots in the graph. To create this dynamic topological graph, we evaluate the visibility of the robot team from a discrete set of observer locations (both adversarial and friendly), and construct a topological graph whose edge weights depend on both adversary position and robot team configuration. We then impose temporal constraints on the evolution of those edge weights based on robot team state and use Mixed-Integer Programming (MIP) to generate optimal multi-robot plans through the graph. The visibility information also informs the lower layers of the autonomy stack to plan minimal visibility paths through the environment for the team of robots. Our approach presents methods to reduce the computational complexity for a team of robots that interact and coordinate across the team to accomplish a common goal. We demonstrate our approach in simulated and hardware experiments in forested and urban environments.

Index Terms—Multi-Robot Coordination, Cooperating Robots, Multi-Robot Systems, Agent-Based Systems.

I. INTRODUCTION

Intelligent planning for collaborative multi-robot teams in complex environments remains a fundamental research problem. Even when restricted to discrete actions and states, the multi-robot Markov decision process can quickly become computationally intractable [1]. This situation is further exacerbated when robot teams must reason about continuous-time dynamics, dynamic obstacles, and complex environmental conditions. In this paper, we discuss our approach, Stratified Topological Autonomy for Long-Range Coordination (STALC), which seeks to develop a unified framework for coordinated motion planning with multi-robot teams. In particular, our approach investigates the problem of minimizing detection and risk when traversing through a potentially hazardous environment. To do this, we developed a hierarchical planning approach that consists of three primary levels: a high-level multi-robot graph planner, a mid-level planner

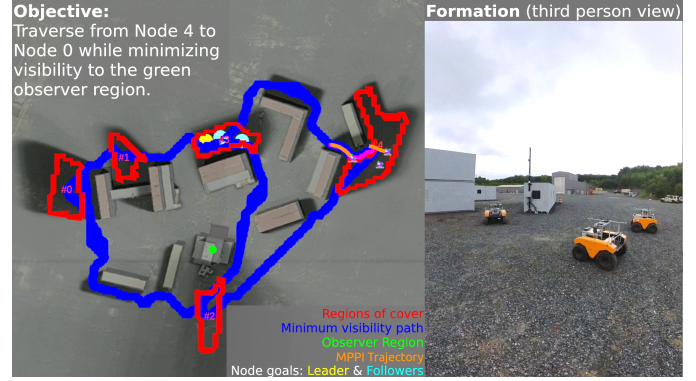


Fig. 1. Experimental operational scenario to minimize visibility while traversing an urban environment. A team of three Clearpath Warthogs navigate the environment while balancing the risk and rewards of moving in formations and providing overwatch for a reconnaissance mission.

for designing low-visibility paths between nodes, and a low-level planner for generating dynamically feasible, collision-free paths for each robot.

Our primary contribution is a graph planning approach using Mixed-Integer Programming (MIP). Our graph planner rapidly solves for a multi-robot plan to efficiently and effectively accomplish a team goal while minimizing visibility to potential observers. We define a *dynamic topological graph*, which embeds the critical features of the planning problem and interactions between robots through a topological graph with dynamic edge costs. We define this graph by segmenting the environment around visibility to potential observers and between teammates. We then capture the relationships between the robots and the environment, defined in the dynamic topological graph, in our MIP formulation. In order to significantly reduce the computational complexity of this type of problem, our approach embeds multi-robot interactions directly in the edge weights instead of defining interactions through a computationally intractable number of variables for each possible state. Additionally, we detail our approach for constructing these dynamic topological graphs using environmental data and our mid-level and low-level planners for executing the multi-agent plans.

To evaluate the effectiveness of our approach, we tested our planner in a series of simulated meadow environments and on hardware in forested and urban environments. In all scenarios, we demonstrate that our planning approach can effectively navigate a team of robots through a complex environment with unified minimum-visibility planning. In an example scenario, Fig. 21 depicts a team of three Clearpath Warthog robots navigating an urban environment.

¹Johns Hopkins University Applied Physics Laboratory, Laurel, MD 20723, USA. Email: Cora.Dimmig@jhuapl.edu, jlmoores@jhu.edu

²Department of Mechanical Engineering, Johns Hopkins University, Baltimore, MD 21218, USA.

³DEVCOM Army Research Laboratory, Adelphi, MD 20783, USA.

Distribution Statement A: Approved for public release. Distribution is unlimited.

This manuscript substantially extends the work in [2] which introduced a method for solving for multi-robot plans on a dynamic topological graph. In the work presented herein, we report algorithms for generating the dynamic topological graph and for utilizing the optimized plans, resulting in a full end-to-end system for multi-robot planning for coordinated maneuvers. In addition, we present hardware experiments that demonstrate our method in real-world environments.

II. RELATED WORK

To address the challenges associated with multi-robot planning in complex environments, researchers have considered many different approaches to multi-robot coordination [3], [4] and cooperative multi-agent planning [1].

In many instances, researchers have addressed the problem of multi-robot coordination or task allocation. Oftentimes, solutions formulate the problem space as a set of discrete actions and states [5]–[9]. This includes conflict-based search methods [10], auction-based methods [11] and game theoretic approaches [12]. However, many of these approaches consider agents independently, ultimately ignoring interactions and cooperation between vehicles. Vehicle interactions can cause the decision space of the problem to grow exponentially, which leads many researchers to consider decomposing the problem into smaller local problems, such as in the game theoretic approach in [13]. Machine Learning (ML) approaches, often using Graph Neural Networks (GNNs) [14], [15], emerge as a way to solve the entire problem end-to-end while considering agent interactions [16] and coordination [17], [18]. However, ML approaches often suffer from poor generalization to environments that were not included in the training distribution and are categorically unable to provide optimality guarantees [16]–[18].

Mixed-Integer Programming (MIP) enables solving for end-to-end optimal solutions and has been studied in a variety of application spaces, including recharging or timed delivery [19], [20], scheduling and task allocation [21], and communication provisioning [22]. However, MIP is NP-complete, leading many approaches to require simplifying heuristics [23] and/or offline computation for optimal solutions [24].

Many researchers have also explored multi-robot motion planning in the context of obstacle avoidance or formation control. For instance, [25] uses MIP and minimum snap trajectories to design collision-free robot trajectories using a GPU. [26] generates a modified version of A* to handle inter-robot constraints. In [27], [28], the authors explore methods for multi-vehicle formation control in the presence of obstacles.

Over the years, some researchers have attempted to provide a unified approach for coordination and control (e.g., [29]–[32]). In many cases, these methods require operating on incredibly simplified and structured environments. In this paper, we propose a unified approach for multi-robot coordination and motion planning through a hierarchical planner, where each layer is informed by the information from the other layers of the hierarchy and our high-level topological graph encodes information about the underlying metric spaces. We then employ a MIP approach to generate coordinated multi-robot plans on the topological graph. In this work, we overcome many of the

computational challenges with MIP-based approaches through a compact multi-agent planning formulation, and we present results rapidly solving end-to-end for optimal solutions.

The most comparable problem formulations to our approach in considering team coordination on graphs include [8] and [18]. In [8], the authors suffer greatly from the curse of dimensionality in the number of agents, reporting that they must decompose the problem into two separate problems and only consider two agents. The authors then present [18], which considers reinforcement learning for team coordination with the intention of addressing the curse of dimensionality. However, their policy for a general graph is limited to ten nodes. When considering training on only one graph, the authors report significant jumps in solution times (on the order of magnitude of minutes, which would be impractical for real-time operation) when considering graphs with 10-25 nodes and only 3-4 agents, additionally in many cases their approach cannot yield a result at all. Our graph planning formulation directly addresses the scalability to large numbers of agents. Furthermore, we present methods to formulate the problem convexly to enable solving for optimal solutions on variable graph sizes in seconds. Due to the computational complexity of this problem space, to the best of our knowledge, there are no reported works with approaches that are capable of computing solutions for the scale of problems we consider.

III. PROBLEM FORMULATION

Our objective is to solve for a multi-robot team plan that minimizes the robot team’s visibility to observers and maximizes safety in an adversarial environment. More specifically, we aim to avoid line-of-sight observations by a static observer in such a way that we proceed tactically from one cover region to another. In addition to minimizing overall visibility, we introduce three foundational robot coordination constructs that we propose as methods to reduce the risk of traversing an adversarial environment:

- **Overwatch:** One team at a protected vantage point over-views the movement of a traversing team to mitigate risk.
- **Formations:** In areas of high vulnerability, moving in a formation increases awareness of the team.
- **Teaming:** Moving as a team in general can provide a higher level of protection to the robots.

We relegate team coordination to planning on a high-level graph, while minimizing visibility and maintaining formation is managed by mid-range and low-level planners, respectively.

IV. STALC TECHNICAL APPROACH

Our technical approach consists of a three-level planning hierarchy including a top-level graph-based planner capable of coordinating multi-robot teams while traversing a hazardous environment. The edges in our graph represent minimally visible paths between the graph’s nodes, which we generate with our mid-level planner using a visibility map and A* search. At the lowest-level, we utilize Model Path Predictive Integral Control (MPPI) [33] to generate local plans, avoid obstacles, and follow the mid-range plan. All three levels share visibility and terrain maps to maintain consistent planning across the hierarchy.

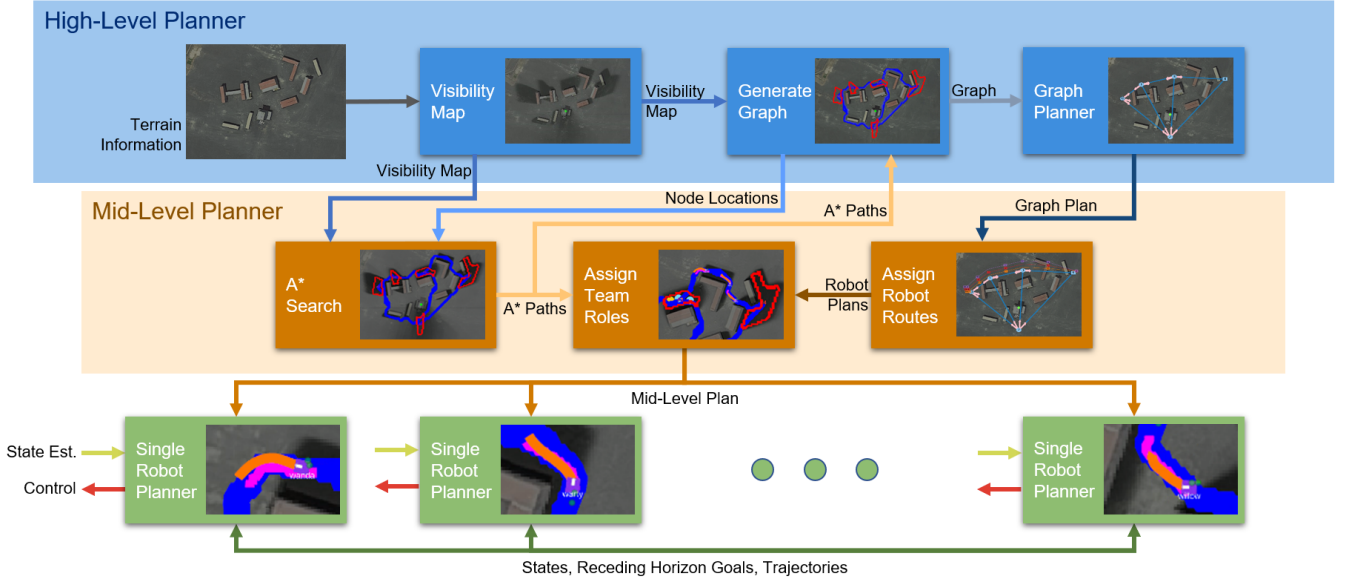


Fig. 2. STALC: Hierarchical planning architecture for a multi-robot team to traverse an environment. The high-level planner segments the environment into a topological graph structure and generates a plan on the graph for the robot team through the environment. The graph construction is informed by the mid-level planner which generates A* paths through the environment. The mid-level planner then takes the output of the graph planner and assigns routes to each robot through the environment. Each group of robots moving together are then assigned roles in their sub-team (i.e., leader or follower). This information is sent to each robot’s low-level planner to generate and execute dynamically feasible, collision-free paths.

Fig. 2 shows a flow diagram of our hierarchical control approach. First, terrain information is used to compute visibility scores, relative to an expected observer distribution, across an area of interest. We use this visibility map to segment the environment into regions of cover (or low visibility), which we use as nodes in a graph structure. We then calculate minimum visibility A* paths between the regions to serve as the edges in the graph. Between each node and edge pair, we compute overwatch scores based on the visibility to the edge from within the node. Together, this information forms a dynamic topological graph for the environment, where the edge weights vary with the state of the robot team. We encode this graph in our MIP graph planner to compute an optimal plan for the multi-robot team. To form our mid-level plan, we assign each robot a route, which corresponds to an A* path, and a role in the team (i.e., leader or follower). Each robot then controls to the A* paths using MPPI in our low-level planner, performs overwatch, and/or moves in formation with their team members. The following sections will outline the algorithms that comprise each block of our overall hierarchical planner.

V. GRAPH GENERATION

A. Visibility Map

To enable low-visibility planning for the multi-robot team, we construct a visibility map. We assume prior knowledge of a Digital Elevation Model (DEM) of the environment and a probability distribution, \mathcal{O} , over \mathbb{R}^3 representing the expected observer position. We do not make assumptions about the form of \mathcal{O} except that we are able to sample from it. In the experimental evaluation that follows, we utilize Gaussian distributions (i.e., $\mathcal{O} \sim N(\mu, \Sigma)$).

For a given DEM and observer distribution, we segment the environment into regions of low and high visibility from the

perspective of the observer. We accomplish this by adapting the notion of a viewshed [34] to the context of a distribution over observer positions. The viewshed of an area is a binary mask marking the regions of a DEM that are visible from a given observer position. Our goal is to estimate the probability that each point in the environment can be seen by the observer.

Taking N samples $\mathcal{o} \sim \mathcal{O}$ from the observer distribution, we compute a viewshed $\mathcal{V}_{\mathcal{o}}$ for each sample. Discretizing the environment into a 2D grid, for each point (x, y) in the environment, the visibility probability is the expectation over the viewsheds from the sampled observer positions. We refer to the map containing the probability of being seen at each point as the *visibility map*. An example of a visibility map is depicted in Fig. 3 with a single observer. The lighter shades represent higher visibility. We formulate the probability of being seen as follows.

$$\mathbb{E}_{\mathcal{o} \in \mathcal{O}}[\mathcal{V}_{\mathcal{o}}(x, y)] \approx \frac{\sum_{i=1}^N \mathcal{V}_{\mathcal{o}_i}(x, y)}{N} \quad (1)$$

The calculation outlined above does not consider the distance from the observer when computing the probability of detection; however, we expect visibility to decrease with increasing distance. To model this effect, we use the distance transform to compute the Euclidean distance from each cell in the map to the nearest observer distribution. For distributions with infinite support, such as a normal distribution, we must choose a “boundary” for the distribution in order to compute the distance transform. In this work, we use the $2\text{-}\sigma$ ellipse. We compute a weight for each cell in the map, such that the probability of detection is 0 beyond the max range and approaches the visibility map value for locations closer to an observer. Thus, we define our visibility map, $\mathcal{P}_{vis}(x, y)$, as

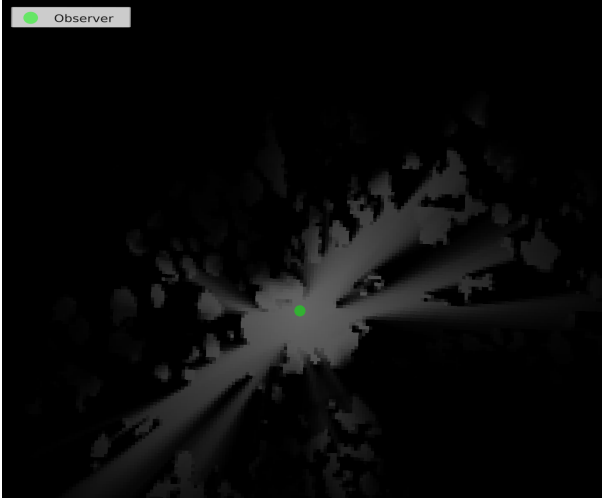


Fig. 3. A visibility map: the observer is positioned in a clearing. The observer distribution is modeled as a normal distribution represented by the green 1- σ ellipse. The gradient in each cell represents the visibility, with lighter being higher visibility.

follows.

$$\mathcal{P}_{vis}(x, y) = \mathbb{E}_{\mathcal{O} \in \mathcal{O}} [\mathcal{V}_{\mathcal{O}}(x, y)] \max \left(1 - \frac{d(x, y)}{d_{max}}, 0 \right) \quad (2)$$

In this calculation, $d(x, y)$ is the distance to the nearest observer and d_{max} is the maximum sight range of the observer.

B. Constructing a Topological Graph

In order to construct a topological graph for planning, we use the visibility map to compute a set of nodes, V , and edges, E , together with a score for the visibility of each edge, represented by a weighted adjacency matrix, W_{vis} . We also compute an overwatch matrix for each node, $W_{ow,v}$ for $v \in V$, which is a weighted adjacency matrix where element $W_{ow,v}(j, k)$ denotes the overwatch that a team of robots positioned at node v can provide for a team traversing edge (j, k) . In Algorithm 1, we present our algorithm to construct the components of the topological graph. The following subsections describe the key steps (represented in the algorithm as functions) in more detail.

1) *ComputeVisibilityMap*: The visibility map computation uses an efficient viewshed algorithm [34] to generate N viewshed maps sampled from the observer distribution \mathcal{O} . We then use equations (1) and (2) to compute the probability of detection for each cell in the map. These calculations form our visibility map \mathcal{P}_{vis} .

2) *ThresholdVisibility*: To identify the regions of low visibility (which we call *cover regions*) from the visibility map, we threshold the map to extract regions below a pre-defined visibility cutoff, ν .

3) *RemoveObstacles*: After thresholding, we additionally remove any regions of the map that are known *a priori* to be non-traversable.

4) *ConnectedComponents*: We then perform a connected-components search to find all the discrete regions whose sizes exceed a threshold value, Ξ_{min} .

Algorithm 1 Topological Graph Construction

Input:

\mathcal{D}	Digital Elevation Model
\mathcal{C}	Obstacle map
\mathcal{O}	Observer distribution
N	Number of samples from observer distribution
ν	Visibility threshold
Ξ_{min}	Minimum cover region size
Ξ_{max}	Maximum cover region size
λ_p	Visibility cost weight

Output:

V	Graph nodes (cover region centroids)
E	Graph edges
W_{vis}	Visibility weight adjacency matrix
$W_{ow,V}$	Overwatch weight matrices for each node $v \in V$

```

1:  $\mathcal{P}_{vis} \leftarrow \text{ComputeVisibilityMap}(\mathcal{D}, \mathcal{O}, N)$ 
2:  $cover \leftarrow \text{ThresholdVisibility}(\mathcal{P}_{vis}, \nu)$ 
3:  $cover \leftarrow \text{RemoveObstacles}(\mathcal{C}, cover)$ 
4:  $regions \leftarrow \text{ConnectedComponents}(cover, \Xi_{min})$ 
5:  $regions \leftarrow \text{SplitRegions}(regions, \Xi_{max})$ 
6:  $V \leftarrow \text{ComputeCentroids}(\mathcal{C}, regions)$ 
7:  $paths \leftarrow \text{ComputePaths}(\mathcal{P}_{vis}, \mathcal{C}, regions, V, \lambda_p)$ 
8:  $\mathcal{N}_{vis} \leftarrow -\log(\max(1 - \mathcal{P}_{vis}, \epsilon))$ 
9:  $n_V \leftarrow \text{Size}(regions)$ 
10:  $W_{vis} \leftarrow \mathbf{0}_{n_V \times n_V}$ 
11:  $E \leftarrow \emptyset$ 
12: for all  $\{(s, g) : path\} \in paths$  do
13:    $W_{vis}[s, g] \leftarrow \text{PathCost}(\mathcal{N}_{vis}, path)$ 
14:    $E \leftarrow E \cup (s, g)$ 
15: end for
16: for  $v \in V$  do
17:    $\mathcal{O}_{ow,v} \leftarrow \text{UniformDistribution}(regions[v])$ 
18:    $\mathcal{P}_{ow,v} \leftarrow \text{ComputeVisibilityMap}(\mathcal{D}, \mathcal{O}_{ow,v}, N)$ 
19:    $\mathcal{N}_{ow,v} \leftarrow -\log(\max(1 - \mathcal{P}_{ow,v}, \epsilon))$ 
20:    $W_{ow,v} \leftarrow \mathbf{0}_{n_V \times n_V}$ 
21:   for all  $\{(s, g) : path\} \in paths$  do
22:      $W_{ow,v}[s, g] \leftarrow \text{PathCost}(\mathcal{N}_{ow,v}, path)$ 
23:   end for
24: end for
25: return  $V, E, W_{vis}, W_{ow,V}$ 

```

5) *SplitRegions*: For some maps and observer positions, the cover regions generated using our method can be large and quite non-convex. Consequently, we enforce a maximum size, Ξ_{max} , for each cover region by iteratively finding the minimum-length cut that divides one region into two smaller ones, where one region has the maximum size [35]. These cuts are repeated until no region is larger than the maximum size.

6) *ComputeCentroids*: The nodes of the topological graph are initially placed at the centroid of each cover region. We then shift them to ensure that the nodes lie inside the cover region (as the centroid could be outside of a non-convex region). Additionally, we ensure the node centers do not collide with any known obstacles. In Fig. 4, we overlay outlines of the cover regions with the visibility map on satellite

Algorithm 2 ComputePaths

Input:

\mathcal{P}_{vis}	Visibility map
\mathcal{C}	Obstacle map
$regions$	Cover regions
V	Graph nodes
λ_p	Visibility cost weight

Output:

$paths$ Map: $(start, goal) \mapsto path$

```
1:  $paths \leftarrow \text{NewMap}()$ 
2:  $is\_start \leftarrow \{v : \text{false} \forall v \in V\}$ 
3:  $is\_goal \leftarrow \{v : \text{false} \forall v \in V\}$ 
4:  $path\_to \leftarrow \{v : \text{null} \forall v \in V\}$ 
5:  $path\_from \leftarrow \{v : \text{null} \forall v \in V\}$ 
6: for all  $s \in V$  do
7:   for all  $g \in V$  do
8:     if  $s = g$  then
9:       continue
10:    end if
11:     $path \leftarrow \text{ComputeSinglePath}(\mathcal{C}, \mathcal{P}_{vis}, s, g, \lambda_p)$ 
12:    if  $\text{PathIsRedundant}(path, s, g)$  then
13:       $path\_to[g] \leftarrow \text{MinCost}(path, path\_to[g])$ 
14:       $path\_from[s] \leftarrow \text{MinCost}(path, path\_from[s])$ 
15:    else
16:       $paths[\{s, g\}] \leftarrow path$ 
17:       $is\_start[s] \leftarrow \text{true}$ 
18:       $is\_goal[g] \leftarrow \text{true}$ 
19:    end if
20:  end for
21: end for
22:  $paths \leftarrow \text{ReconnectNodes}(is\_start, is\_goal,$ 
    $path\_from, path\_to)$ 
23: return  $paths$ 
```

imagery of the environment.

7) *ComputePaths*: We define the algorithm for computing paths between cover regions in Algorithm 2. In particular, we generate a mapping $paths$ that stores the path between any two start and goal nodes. We initialize this mapping with the *NewMap* function.

8) *ComputeSinglePath*: To identify redundant edges and compute the edge weights for the graph, we use an optimal path planning algorithm to compute a path between each pair of nodes in the graph. In this work, we use a standard A* search where the heuristic cost, $h(b)$, is the Euclidean distance from the current position to the goal, $g(b)$ denotes the cost to follow the optimal path from the start to b , and the successor cost, $c(b, b')$, is the cost to go from a cell in the map to a neighbor, with terms incorporating both the distance and the detection probability.

$$c(b, b') = \|b - b'\|(1 + \lambda_p \mathcal{N}_{vis}(b')) \quad (3)$$

$$g(b') = g(b) + c(b, b') \quad (4)$$

In (3), λ_p is a scaling factor to weight the contribution of the visibility cost. Since the true cost-to-go is equal to the heuristic

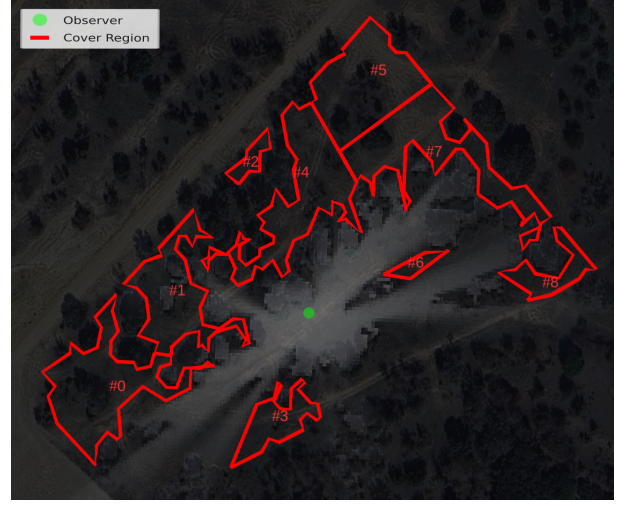


Fig. 4. A visibility map overlaid on satellite imagery of the environment: cover regions are outlined in red and node numbers are located within the regions near the centroid of each region.

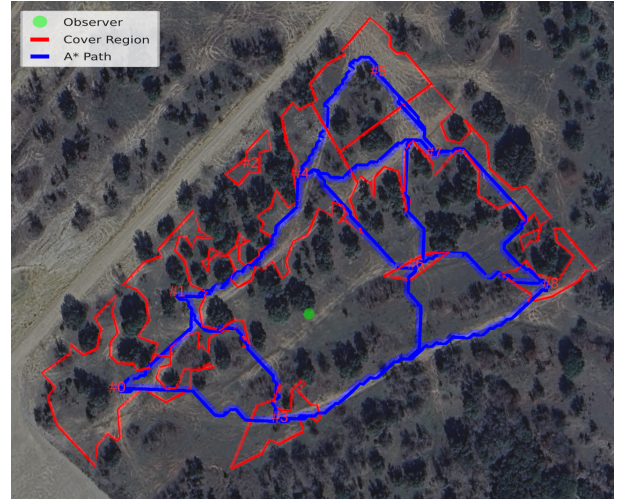


Fig. 5. Pruned A* paths between regions of cover.

cost plus a non-negative visibility term, the heuristic $h(b)$ is trivially admissible.

9) *PathIsRedundant*: When computing the set of graph edges and the cost to traverse each edge, we initially consider the topological graph to be fully-connected. In order to reduce the number of edges considered in the graph planner (Sec. VI), we prune the graph by eliminating redundant edges. A redundant edge is any edge connecting node v_i to node v_j where the optimal path from v_i to v_j passes through a cover region associated with another node $v_k \notin \{v_i, v_j\}$. Whenever a redundant edge is removed, we compare the cost of the corresponding path with both the current minimum cost redundant path starting at v_i and the current minimum cost redundant path ending at v_j using the function *MinCost* and save the lower cost paths for later use in *ReconnectNodes*.

10) *ReconnectNodes*: In rare circumstances, the pruning step leaves a node without any connections to the graph. In this case, we restore the lowest cost edge for which the disconnected node is a start node and the lowest cost edge

where it is a goal node. An example of the pruned A* paths is shown in Fig. 5.

11) *PathCost*: When traversing a path, $B = \{b_1, b_2, \dots, b_n\}$, $b_i = [x_i, y_i]^T$, through the environment, we consider the total probability of non-detection, P_{nd} , as the product of the probabilities of non-detection at each cell (assuming independence). This can be calculated for a visibility map \mathcal{P}_{vis} or overwatch map $\mathcal{P}_{ow,v}$, so we use a general \mathcal{P} in our equations.

$$P_{nd} = \prod_{b \in B} (1 - \mathcal{P}(b)) \quad (5)$$

Taking the negative log of this quantity, we find that we can compute a negative log non-detection probability by summing the contributions of each cell along the path.

$$-\log(P_{nd}) = \sum_{b \in B} -\log(1 - \mathcal{P}(b)) \quad (6)$$

As the probability of detection approaches one, the cost to traverse a cell approaches infinity. In order to avoid infinite values in the optimization problem, we bound the maximum probability of detection at each cell to $1 - \epsilon$ (for a small positive ϵ). We call the map containing the negative log non-detection probabilities at each cell \mathcal{N} , or \mathcal{N}_{vis} for visibility and $\mathcal{N}_{ow,v}$ for overwatch.

In the final step of the path cost calculation, we compute the weight for each edge $e = (v_1, v_2)$ that remained after the pruning step by considering the optimal path B_e .

$$W(v_1, v_2) = \sum_{b \in B_e} \mathcal{N}(b) \quad (7)$$

12) *Overwatch Opportunities*: An overwatch opportunity represents the ability of a subset of robots in a cover region to provide support to another team as they traverse an edge in the graph. The process of computing an overwatch weight matrix, $W_{ow,v}$, which represents the benefit of performing overwatch, is very similar to the visibility map calculation; however, instead of sampling from the observer distribution, we sample uniformly from the cover region associated with the node v . We sample uniformly since we have hard boundaries for the cover region, whereas in the case of the observer, we may not know the boundaries, so we considered a Gaussian distribution. We call the uniform distribution associated with the node v cover region $\mathcal{O}_{ow,v}$. This distribution is formed with the function *UniformDistribution*. Using this distribution, we produce a visibility map for an observer located at node v , which we call an *overwatch map*, $\mathcal{P}_{ow,v}$. We then apply equations (6) and (7) to $\mathcal{P}_{ow,v}$ to compute the overwatch score for each edge in the graph. We perform this calculation for each node resulting in a series of overwatch weight matrices $W_{ow,V}$ to be used in our topological graph. An example overwatch map is shown in Fig. 6.

C. Topological Graph Refinement

We graphically depict the information embedded in our topological graph through the schematic representation shown in Fig. 7. The graph includes nodes for each cover region,

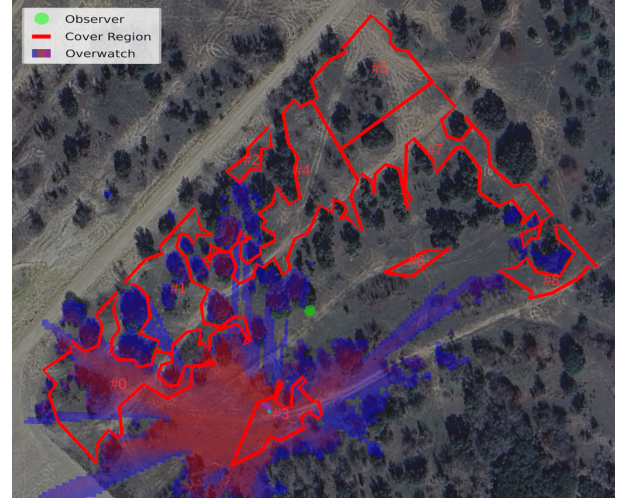


Fig. 6. The overwatch map from node 3. Pink and red shading denotes areas of high overwatch potential, blue regions have lower overwatch potential, and unshaded areas have none.

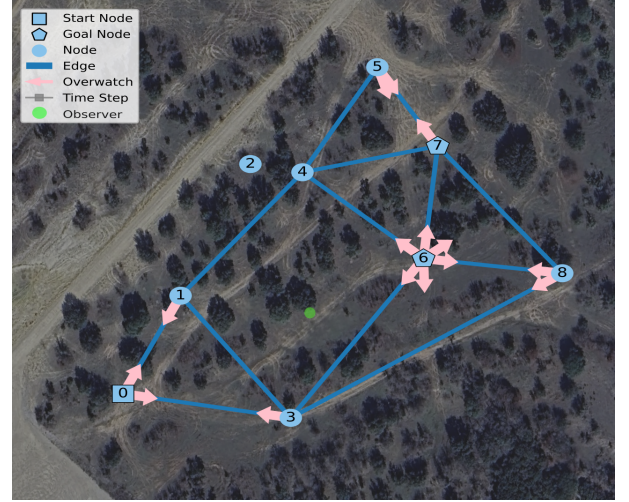


Fig. 7. Schematic topological graph with overwatch opportunities indicated by arrows pointing from the overwatch node to edges that can be observed.

edges representing the pruned A* paths, and overwatch opportunities from the overwatch maps, denoted by arrows from the overwatch node to the edge that can be monitored.

When transforming the environment segmentation into this schematic representation, we use heuristics to refine the graph based on the robots' capabilities and the priorities of the scenario. In particular, we set a maximum distance that can be traversed and remove edges from E that do not meet this threshold. When necessary due to a particular scenario, we add vulnerable edges to nodes that became isolated from the maximum distance threshold by adding back the lowest-cost edge to E .

We add overwatch opportunities from $W_{ow,V}$ to our graph when a robot from a node can provide support to the robot(s) traversing an edge. To determine which overwatch opportunities are valuable to the planning problem, we enforce overwatch heuristics based on the scenario. First, we impose a maximum overwatch distance (e.g., due to sensor constraints)

by checking the distance to each end point of an edge. We then add a scale factor to the overwatch weights based on the priorities of the scenario (e.g., if overwatch is more or less valuable). We consider providing overwatch to offer a cost reduction to traverse an edge, so we bound the ratio between the overwatch reduction and edge weight. Typically, we set these bounds to saturate at a 90% cost reduction due to overwatch (such that traversing an edge is never without cost) and we only consider the overwatch opportunity if it provides minimally a 40% cost reduction (based on what is considered worthwhile in the scenario). These thresholds and the scale factor on overwatch would be set based on the priorities of the scenario and we demonstrate different values for these parameters in our analysis.

VI. GRAPH PLANNER

To solve for an optimal plan for a team of robots to navigate an environment while optimizing for our scenario objectives, we developed a MIP approach to capture the relationships in our topological graph. In particular, we consider our graph to be a *dynamic* topological graph, as it explicitly embeds the dynamic state of the robot team in the edge costs in the formulation of our optimization problem.

A. Mixed-Integer Programming Approach

In order to encode the dynamic topological graph structure in our MIP problem, we define decision variables that track the number of robots at each location (node or edge) in the graph. We then constrain the robots' movement to the graph structure by considering the flow of robots between nodes and edges. We consider graph $G = (V, E, W_E)$ with nodes $v \in V$, edges $e \in E$, and edge costs $w_e \in W_E : E \times X \rightarrow \mathbb{R}_{>0}$. The edge costs w_e depend on the costs from the visibility map (W_{vis}), overwatch opportunities ($W_{ow,V}$), and the state of the robot team on the graph $x \in X$, where $X = \{p_{e_1}, p_{e_2}, \dots, p_{e_{n_E}}\}$ and $p_{e_j} \in \mathbb{Z}_{>0}$ is the number of robots on edge e_j . We consider a fixed time horizon $t \in [1, n_T]$. Our overall objective is to position a team of robots at a set of target locations within this time horizon while minimizing time and visibility due to traversing by using our constructs defined in Sec. III. Thus, we define cost functions for the cost of traversing $C_{W_{e,t}}$ (based on the edge weights on the graph and reductions due to moving as a team), the cost reduction from overwatch $C_{\Omega_{o,t}}$, and a cost for time C_{T_t} . Our cost functions depend on the positions of the robots relative to their teammates and reflect the dynamic element of the topological graphs. Specifically, the overall cost to traverse the graph decreases when the conditions for overwatch, moving in formation, or other general teaming are met.

We express a general form of our problem as follows, where we define an indicator function χ , which checks that the state of the robot team is constrained to the graph structure, and starts and ends at positions defined by the sets S and D .

$$\min \sum_{t=1}^{n_T} \left(C_{T_t} + \sum_{e \in E} C_{W_{e,t}} + \sum_{o \in O} C_{\Omega_{o,t}} \right) \quad (8)$$

$$\text{s.t. } \chi(x, G, S, D) = 1 \quad (9)$$

TABLE I
MIP PARAMETERS

Category	Var	Description
Problem Size	n_A	Number of agents/robots
	n_T	Number of time steps in the time horizon
	n_O	Number of overwatch opportunities
	n_E	Number of edges, both directions
	n_V	Number of nodes/vertices
	n_L	Number of locations ($n_E + n_V$)
	n_S	Number of start locations
Scenario Variables	n_G	Number of goal locations
	E	Set of edges e
	V	Set of nodes/vertices v
	L	Set of locations l consisting of edges and vertices, $E \cup V$
	S	Set of start locations s , $S \subseteq L$
	D	Set of goal/destination locations d , $D \subseteq L$
Problem Parameters	O	Set of overwatch opportunities o , (v_i, e_j) where node v_i can overwatch edge e_j
	t	Time step from 1 to n_T
	n_s	Number of robots at start location $s \in S$
Cost of Traversing	n_d	Number of robots at goal location $d \in D$
	w_e	Base cost to traverse edge $e \in E$
	a_e	Minimum desired number of robots on e
	m_e	Additional cost for robots on e before a_e
Cost of Overwatch	r_e	Cost reduction on e for robots over a_e
	ω_o	Benefit of full overwatch for $o \in O$
	α_o	Number of robots for full overwatch for o
	γ_o	Reward for overwatch robots over α_o for o

In the following sections we expand on this formulation, defining specific cost functions and constraints. We consider a reconnaissance test scenario, however the algorithmic developments presented in this paper could be applied to a wide variety of scenarios.

A key innovation of this method is our ability to remove the standard dependence on the number of robots. Instead of tracking each robot's path through the graph, we track the total number of robots at each node in the graph at each time step. This formulation abstracts away the assignment of paths for individual robots to a rapid post-processing step, ultimately significantly improving computation times. Furthermore, this formulation is flexible to a varying number of robots.

We define the parameters that we use to formulate the multi-robot MIP in Table I and the decision variables in Table II. Furthermore, we specify the constraints for the lower bounds (LB) and upper bounds (UB) of our decision variables in Table II.

B. Key Formulation Innovations

We apply three core innovations to preserve linearity in our expression of the MIP and significantly improve computation time: our integer decision variable formulation, utilization of indicator variables, and methods for maintaining convexity in our cost functions.

1) *Integer Decision Variable Formulation:* Common formulations for multi-agent problems consider all possible states

TABLE II
MIP DECISION VARIABLES (AT TIME t)

Var	Type	LB	UB	Description
$p_{l,t}$	Integer	0	n_A	Number of robots at location l
$\phi_{e,t}$	Binary	0	1	Whether robots are on edge e
ψ_t	Binary	0	1	Whether robots have moved
$\check{C}_{We,t}$	Cont.	0	∞	Cost of traversing edge e
$\check{C}_{\Omega o,t}$	Cont.	$-\infty$	0	Cost of overwatch opportunity o

of robots at locations in the graph across all time steps. This is $n_T n_L^{n_A}$ possible states. In a MIP formulation, enumerating these states as binary decision variables would be computationally intractable. Another common formulation is to encode each robot's location at each time step. This enumerates as $n_T n_L n_A$ total variables which is also highly computationally intensive for large numbers of agents and locations.

We drastically reduce the size of the decision space by instead considering how many robots are at each location at each time step with $n_T n_L$ integer variables. This still allows us to analyze interactions between robots sharing edges or providing overwatch, but eliminates the exponential growth of the decision space. This formulation obfuscates the paths of each individual robot in the optimization program, though they can easily be assigned afterwards. Additionally, the paths can be ensured to follow the topology of the graph through sequential flow constraints considering the movement of all robots, which we present in the following sections.

With this formulation, we embed the multi-robot interactions directly in the edge weights of our dynamic topological graph. In particular, we consider benefits from moving in formations and as a team to directly scale with the number of robots on an edge; thus our choice of decision variable greatly simplifies these calculations. For interactions through overwatch opportunities, we define costs and constraints for each overwatch opportunity that depend on the number of robots at the overwatch nodes and related edges to reduce the cost of traversing those edges. Fully defining each of these possible interactions when instead enumerating variables for each robot would significantly increase the problem's complexity. Our choice of decision variables is pivotal to keeping the problem computationally tractable in a complex decision space.

2) *Indicator Variables*: To maintain linearity in our problem formulation, we add binary, or indicator, decision variables when necessary using the following form.

Proposition 1. For $b \in [0, b^\top]$, an indicator variable $\alpha \in \{0, 1\}$ can be expressed as follows, for any constant $a \geq 0$.

$$\alpha = \begin{cases} 1, & b > 0 \\ 0, & b = 0 \end{cases} \Leftrightarrow \min a\alpha \text{ s.t. } \alpha \geq \frac{b}{b^\top} \quad (10)$$

We can then use the newly created binary variable α in our cost functions and constraints. As long as α is used in contexts that will be minimized, the value of α will be strict to the piecewise expression in (10). This is due to the formulation;

α can only be 0 or 1, and the constraint follows that $\frac{b}{b^\top} > 0$ for $b > 0$ and $\frac{b}{b^\top} = 0$ for $b = 0$. For α to be minimized means that the associated cost function has the lowest value when $\alpha = 0$ (compared to $\alpha = 1$). Indicator variables of this form can aid in expressing complex equations more efficiently and effectively in our optimization problem.

3) *Convex Cost Functions*: We aim to express our costs and constraints convexly, since convex cost functions can significantly improve the computation time of an optimization program. In particular, since we are using MIP, we want to formulate our cost functions to be convex when our integrality constraints are relaxed. For brevity, when we refer to the convexity of a function, we are considering the convexity when the integrality constraints are relaxed.

To produce a convex and positively homogeneous function, we can form a *perspective function*, as originally presented in [36]. In particular, we utilize the following result from [37], where $\mathbb{R}_{>0}$ is the set of positive real numbers.

Proposition 2. Let $f : \mathbb{R}^n \rightarrow [-\infty, \infty]$. Then, the perspective function \tilde{f} is convex if and only if f is convex.

$$\tilde{f}(x, y) = yf\left(\frac{x}{y}\right), \quad x \in \mathbb{R}^n, y \in \mathbb{R}_{>0} \quad (11)$$

The following example from [38] shows a perspective function in practice.

Example 1. For $y \geq 0$, the perspective function of the convex function $f(x) = \|Ax + b\|$ is given by $\tilde{f}(x, y) = \|Ax + by\|$, where $x \in \mathbb{R}^n$, $A \in \mathbb{R}^{n \times n}$, $b \in \mathbb{R}^n$. \tilde{f} is jointly convex in x and y by Proposition 2.

In this work, we formulate our cost functions as piecewise functions based on the different regimes of operating alone or with a team. Using perspective functions, we can derive convex piecewise cost functions. This allows us to express these complex functions compactly through a linear cost term with linear constraints as follows.

Proposition 3. If $f(x)$ is a convex piecewise linear function with constraints $c_1(x), \dots, c_n(x)$, then the following are equivalent for some auxiliary variable \check{f} .

$$\min f(x) \Leftrightarrow \min \check{f} \text{ s.t. } \check{f} \geq c_1(x), \dots, \check{f} \geq c_n(x) \quad (12)$$

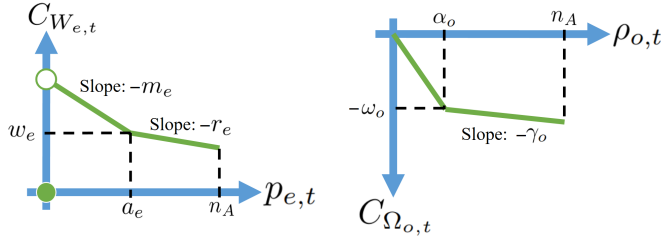
C. MIP Cost Function

Using the information embedded in our dynamic topological graph and the innovations described above, we generate cost functions to minimize the overall cost of traversing and the total time to reach a set of target locations.

1) *Cost of Traversing*: We formulate a cost of traversing with three main components: (a) edge cost, (b) vulnerability cost and (c) teaming rewards. Using the parameters from Table I, our edge cost is the positive valued w_e for a team of robots to traverse edge e . For particularly vulnerable edges, it is desired for more agents to move together across the edge to enable moving in a formation for greater awareness. Thus, for each edge, to encode vulnerability, a minimum desired

number of robots a_e to traverse the edge is specified and an additional positive cost m_e is incurred for each robot until the minimum is met. Finally, we consider an incentive for further teaming through positive rewards r_e for additional robots moving together over the minimum desired. These components comprise the piecewise-linear cost of traversing an edge at a particular time, $C_{W_{e,t}}$, which can be expressed as a function of the number of robots on the edge at that time, $p_{e,t}$. This cost function is depicted in Fig. 8a.

$$C_{W_{e,t}} = \begin{cases} 0, & p_{e,t} = 0 \\ w_e + m_e(a_e - p_{e,t}), & 0 < p_{e,t} \leq a_e \\ w_e - r_e(p_{e,t} - a_e), & a_e \leq p_{e,t} \leq n_A \end{cases} \quad (13)$$



(a) Cost of traversing edge e at time t versus number of robots on the edge (b) Cost of overwatch opportunity o at time t versus number of overwatch robots

Fig. 8. Piecewise-Linear Cost Functions

To reduce computation time, we want a convex formulation of this cost function. The cost in (13) will not be convex in this case due to the zero point. To restate this cost, we first add an indicator variable for whether an edge is used, $\phi_{e,t}$, using Proposition 1. We then consider the function $f(p_{e,t}) = w_e + m_e(a_e - p_{e,t})$, which is convex when we select $m_e \geq r_e$. Using Proposition 2, we can state the perspective function of $f(p_{e,t})$.

$$\tilde{f}(p_{e,t}, \phi_{e,t}) = -m_e p_{e,t} + (w_e + m_e a_e) \phi_{e,t} \quad (14)$$

By Proposition 2, the perspective function, $\tilde{f}(p_{e,t}, \phi_{e,t})$, is a convex function in $p_{e,t}$ and $\phi_{e,t}$. Additionally, when $p_{e,t} = 0$ then $\phi_{e,t} = 0$ by definition, and this cost is zero. Otherwise, for any $p_{e,t} > 0$ then $\phi_{e,t} = 1$ and $\tilde{f}(p_{e,t})$ is identical to the second case in (13). Thus, this new function combines the first two cases in (13) and results in a convex piecewise linear function as follows.

$$C_{W_{e,t}} = \begin{cases} -m_e p_{e,t} + (w_e + m_e a_e) \phi_{e,t}, & 0 \leq p_{e,t} \leq a_e \\ w_e - r_e(p_{e,t} - a_e), & a_e \leq p_{e,t} \leq n_A \end{cases} \quad (15)$$

Due to the convexity of this function, we can equivalently express this cost in our optimization problem with a linear term in the cost function that scales with our decision variables $\tilde{C}_{W_{e,t}}$ and two linear constraints, as described in Proposition 3.

$$\tilde{C}_{W_{e,t}} \geq -m_e p_{e,t} + (w_e + m_e a_e) \phi_{e,t} \quad (16)$$

$$\tilde{C}_{W_{e,t}} \geq -r_e p_{e,t} + (w_e + r_e a_e) \phi_{e,t} \quad (17)$$

These constraints are for the two line segments seen in Fig. 8a. We utilize $\phi_{e,t}$ in (17), so that this term is defined whenever there are vehicles traversing and is zero otherwise. This sets the minimum value of the cost $\tilde{C}_{W_{e,t}}$ to zero when

vehicle's are not traversing edge e at time t . Since we are optimizing for minimum cost, $\tilde{C}_{W_{e,t}}$ will be tight to the piecewise-linear cost function (15).

2) *Cost of Overwatch*: When an edge can be monitored from a node, we consider this an overwatch opportunity and having overwatch while traversing can offer a cost reduction. When robots are traversing a corresponding edge, any number of robots at an overwatch node results in overwatch, but more robots may provide a greater reward. Using the parameters from Table I, we specify a positive ω_o as the benefit of overwatch opportunity o , α_o is the number of robots needed for full overwatch (i.e., to receive the full reward), and a positive γ_o is a further reward for additional robots past α_o (i.e., a further teaming incentive). We consider $\rho_{o,t}$ to be the number of overwatch robots for opportunity o at time t . Thus, as depicted in Fig. 8b, for a particular overwatch opportunity the “cost” is $C_{\Omega_{o,t}}$.

$$C_{\Omega_{o,t}} = \begin{cases} -\frac{\omega_o}{\alpha_o} \rho_{o,t}, & 0 \leq \rho_{o,t} \leq \alpha_o \\ -\omega_o - \gamma_o(\rho_{o,t} - \alpha_o), & \alpha_o \leq \rho_{o,t} \leq n_A \end{cases} \quad (18)$$

This “cost” will always be negative since it is rewarding overwatch. Similarly to the cost for traversing, since this piecewise-linear cost is convex when integrality constraints are relaxed and $\omega_o/\alpha_o \geq \gamma_o$, we can express the cost with a decision variable, $\tilde{C}_{\Omega_{o,t}}$, that enters linearly in our cost function with two linear constraints.

$$\tilde{C}_{\Omega_{o,t}} \geq -\frac{\omega_o}{\alpha_o} \rho_{o,t} \quad (19)$$

$$\tilde{C}_{\Omega_{o,t}} \geq -\omega_o - \gamma_o(\rho_{o,t} - \alpha_o) \quad (20)$$

We utilize the overwatch robot variables, $\rho_{o,t}$, for ease of formulation, but can restate these constraints without these additional variables in order to reduce overall computation time for the optimization problem. For a particular $o \in O$, we consider the number of robots providing overwatch to be equal to the number of robots at the node, v_i , if there are robots on the edge, e_j . We set $\rho_{o,t} = p_{v_i,t}$, resulting in the following constraints.

$$\tilde{C}_{\Omega_{o,t}} \geq -\frac{\omega_o}{\alpha_o} p_{v_i,t} \quad (21)$$

$$\tilde{C}_{\Omega_{o,t}} \geq -\omega_o - \gamma_o(p_{v_i,t} - \alpha_o) \quad (22)$$

To ensure there are robots traversing the corresponding edge e_j , we add another constraint dependent on $p_{e_j,t}$.

$$\tilde{C}_{\Omega_{o,t}} \geq -\frac{\omega_o}{\alpha_o} n_A p_{e_j,t} \quad (23)$$

This constraint has a steeper slope (due to scaling by n_A) than (21) and (22) when there are robots on the edge (i.e., when $p_{e_j,t} > 0$), to ensure it is the least restrictive (which we can guarantee for convex (18)). When there are robots at the node and there are not robots on the edge (i.e., $p_{v_i,t} > 0$ and $p_{e_j,t} = 0$), (23) is the most restrictive overwatch constraint. This forces the cost $\tilde{C}_{\Omega_{o,t}}$ to be zero, since there is not a benefit from overwatch when there are not robots traversing the edge. Similarly, when $p_{v_i} = 0$, $\tilde{C}_{\Omega_{o,t}} = 0$ since there are not robots providing overwatch.

3) *Cost of Time*: The final cost we consider, C_{T_t} , is for minimizing the time to achieve the goal. We formulate a cost that scales with time and is multiplied by the binary decision variables ψ_t that represent whether robots have moved at time t . Thus, this cost is an incentive to achieve the goal as quickly as possible, since the total cost would be smallest when the robots accomplish the goal in minimal time. We define this cost for all time t .

$$C_{T_t} = t\psi_t \quad (24)$$

4) *Overall Objective Function*: When we combine all of the cost terms, we express our overall objective function to minimize as follows.

$$C = \sum_{t=1}^{n_T} \left(C_{T_t} + \sum_{e \in E} \check{C}_{W_{e,t}} + \sum_{o \in O} \check{C}_{\Omega_{o,t}} \right) \quad (25)$$

A weight can be added to each term in (25) depending on the priority of a particular scenario (e.g., minimizing traversing cost versus minimizing time).

D. MIP Constraints

We add constraints to set support variables used in our cost functions and to restrict movement to the dynamic topological graph.

1) *Edge Used Variables*: We utilize binary variables $\phi_{e,t}$ that track if an edge is used in Section VI-C1. We set $\phi_{e,t}$ to true if there are robots on edge e at time t and false otherwise through the following constraint.

$$\phi_{e,t} \geq \frac{1}{n_A} p_{e,t} \quad (26)$$

This constraint follows the form in Proposition 1 and $\phi_{e,t}$ is utilized in cases where cost is minimal when $\phi_{e,t} = 0$.

2) *Time Tracking Variables*: We add binary variables, ψ_t , to track if there are robots on the edges of the graph, to use in the time cost function in (24). Again we use the form in Proposition 1, but instead of for a single variable, we are considering the sum of the number of robots on edges at each time step. This sum tracks whether robots are still moving since robots cannot go instantaneously between nodes. Additionally, this formulation assumes that traversing edges has cost and remaining at nodes does not, such that remaining on an edge would not provide a benefit. Following Proposition 1, ψ_t only contributes to increasing the overall cost in (24). For each time step t , we bound ψ_t .

$$\psi_t \geq \frac{1}{n_A} \sum_{e \in E} p_{e,t} \quad (27)$$

3) *Start Locations*: We add constraints for the start locations of each robot. For each start location $s \in S$, with n_s robots at that location, we add the following constraint.

$$p_{s,1} = n_s \quad (28)$$

4) *Goal Locations*: For each goal location, or destination, $d \in D$, we set the minimum number of robots required at that location, n_d robots, through the following constraint.

$$p_{d,n_T} \geq n_d \quad (29)$$

5) *Maximum Robots*: We bound the total number of robots across all locations of the graph for each time t .

$$\sum_{l \in L} p_{l,t} = n_A \quad (30)$$

6) *Sequential Flow*: We add a sequential flow constraint to ensure that movement across the graph is restricted to the structure of the graph. In particular, for each node, the number of robots in the node and flowing into the node must be equal to the number of robots in the node and flowing out of the node in the next time step. Thus, for each time $t \in [2, n_T]$ and node v_j , we add the following constraint.

$$\sum_{l_{ij}=(v_i,v_j) \in L} p_{l_{ij},t-1} = \sum_{l_{ji}=(v_j,v_i) \in L} p_{l_{ji},t} \quad (31)$$

The first sum considers all locations of the form $l_{ij} = (v_i, v_j)$ and the second sum considers all locations of the form $l_{ji} = (v_j, v_i)$ for a fixed node v_j . Both sets of locations include l_{jj} since all nodes have self-loops. This constraint assumes a robot would never stay on an edge (due to the cost). This is enforced by the cost function as long as the cost of all edges is greater than zero and overwatch is never provided from an edge. This constraint allows robots to move from one edge to the next without stopping at the node.

7) *Negative Edge Weights*: We add a constraint to ensure that edge weights do not become negative due to the reductions from overwatch opportunities. For each edge and time step, we add the following constraint.

$$\check{C}_{W_{e,t}} + \sum_{o=(v_i,e) \in O} \check{C}_{\Omega_{o,t}} \geq \phi_{e,t} \quad (32)$$

When the edge is used ($\phi_{e,t} = 1$), this constraint ensures that the minimum cost associated with the edge is 1, and otherwise 0. The cost is strict to this bound since we are minimizing costs. This constraint is only necessary for edges that can be monitored through overwatch and can be omitted for the other edges if there are checks in place for the relative values of the edge weight to teaming benefits.

E. MIP Optimization Problem

Combining our objective function and constraints from the previous sections, our overall MIP optimization problem is expressed in Table III.

By employing our key formulation innovations from Sec. VI-B, we can use mixed-integer *linear* programming to solve our problem since we have a linear objective function with linear constraints.

We solve the optimization program shown in Table III using the Gurobi optimizer [39].

F. MIP Problem Formulation Considerations

We formulate our optimization problem such that edges have cost and nodes do not. In particular, we assure that there is not a benefit to staying on an edge, such that any movement on edge (and associated cost accrual) is necessary to achieve the overall objective. However, remaining at a node could provide a benefit, such as to enable performing overwatch of

TABLE III
MIP OPTIMIZATION PROBLEM

Optimization Problem		Eq.
$\min \sum_{t=1}^{n_T} \left(C_{T_t} + \sum_{e \in E} \check{C}_{W_{e,t}} + \sum_{o \in O} \check{C}_{\Omega_{o,t}} \right)$ subject to		(25)
Cost Constraints	$\check{C}_{W_{e,t}} \geq -m_e p_{e,t} + (w_e + m_e a_e) \phi_{e,t},$	$\forall e, t$ (16)
	$\check{C}_{W_{e,t}} \geq -r_e p_{e,t} + (w_e + r_e a_e) \phi_{e,t},$	$\forall e, t$ (17)
	$\check{C}_{\Omega_{o,t}} \geq -\frac{\omega_o}{\alpha_o} p_{v_i,t},$	$\forall o, t$ (21)
	$\check{C}_{\Omega_{o,t}} \geq -\omega_o - \gamma_o (p_{v_i,t} - \alpha_o),$	$\forall o, t$ (22)
	$\check{C}_{\Omega_{o,t}} \geq -\frac{\omega_o}{\alpha_o} n_A p_{e_j,t},$	$\forall o, t$ (23)
Constraints	$\phi_{e,t} \geq \frac{1}{n_A} p_{e,t},$	$\forall e, t$ (26)
	$\psi_t \geq \frac{1}{n_A} \sum_{e \in E} p_{e,t},$	$\forall t$ (27)
	$p_{s,1} = n_s,$	$\forall s$ (28)
	$p_{d,n_T} \geq n_d,$	$\forall d$ (29)
	$\sum_{l \in L} p_{l,t} = n_A,$	$\forall t$ (30)
	$\sum_{l_{ij}=(v_i,v_j) \in L} p_{l_{ij},t-1} = \sum_{l_{ji}=(v_j,v_i) \in L} p_{l_{ji},t},$	$\forall v_j, t \in [2, n_T]$ (31)
	$\check{C}_{W_{e,t}} + \sum_{o=(v_i,e) \in O} \check{C}_{\Omega_{o,t}} \geq \phi_{e,t}$	$\forall e, t$ (32)

other traversing team members. This assumption is built into the problem's formulation.

We assume a graph without negative cycles. Overwatch for one edge can come from multiple nodes, but the weight of the edge (resulting from the cost of traversing, benefit of overwatch, and cost reductions from vulnerability/teaming) cannot reduce to 0 or below. We perform checks on the overwatch reductions to ensure that these conditions are met. Additionally, we add the constraint in equation (32) to bound the edge weights. The formulation proposed herein allows robots at one node to overwatch robots traversing multiple edges. Intuitively, for an overwatch opportunity to be used, the cost reduction from overwatch needs to be more than the cost to get to the overwatch position. Otherwise, the robots will stay together for teaming benefits.

While our solutions are always guaranteed to be optimal, the optimal solution is not guaranteed to be unique. Small problems with simple numbers can result in many equivalent cost solutions and cause computation time to increase. For example, with teaming, without any other factors such as vulnerability and overwatch, if the r_e cost reductions are equivalent on all edges and there are multiple routes being taken, more robots will go on the longest route, which is logical from a risk mitigation perspective. If route lengths are equal, multiple optimal solutions will arise. We demonstrate simple simulated scenarios where this is more of a consideration than in our hardware experiments where we utilize our environment segmentation approach.

VII. MID-LEVEL PLANNER

Our mid-level planner takes the output from the MIP problem, determines between which nodes each robot is intended

to traverse and generates minimally visible paths to follow.

A. Robot Route Assignment

After generating an optimal plan from our optimization problem in Table III, we use the resulting decision variable $p_{l,t}$ in an assignment routine to determine the routes for each robot through the graph. We use each start location from our set S and then go to locations in the form (v_1, v_2) . At each time step, we assign a robot to a location with a start point, v_1 , that matches their current end point, v_2 , to maintain movement along the graph. For a node, the start and end points are equal (i.e., $v_1 = v_2$). We do this for each robot until all robots have a route through the graph. We present Algorithm 3 with the details of this assignment process. We define the following functions for our algorithm: *NewList()* to create a new empty list, *RemoveItem(S)* to remove an item from set S (and output that item), and *AddItem(m)* to add item m to an existing list. Tracking the number of robots at each location rather than routes for each robot directly necessitates this post-processing step, however the paradigm shift to integer decision variables (as described in Sec. VI-B1) enables a significant reduction in computational complexity by removing the dependence on the number of robots in the size of our decision space.

Algorithm 3 Robot Route Assignment

Input:

- $p_{l,t}$ Number of robots at location l at time t ,
 $\forall l \in L, t \in [1, n_T]$
- S Set of n_A start locations
- n_A Number of agents/robots
- n_T Number of time steps

Output:

- M List of routes for each robot ($M_a \forall a$)

```

1:  $M \leftarrow \text{NewList}()$ 
2: for all  $a \in [1, n_A]$  do
3:    $M_a \leftarrow \text{NewList}()$ 
4:    $s_a \leftarrow \text{RemoveItem}(S)$ 
5:    $M_a \leftarrow \text{AddItem}(s_a)$ 
6:    $p_{s_a,1} \leftarrow p_{s_a,1} - 1$ 
7:    $(n_1, n_2) \leftarrow s_a$ 
8:   for all  $t \in [2, n_T]$  do
9:     for all  $l \in L$  do
10:      if  $p_{l,t} > 0$  then
11:         $(v_1, v_2) \leftarrow l$ 
12:        if  $n_2 = v_1$  then
13:           $M_a \leftarrow \text{AddItem}(l)$ 
14:           $p_{l,t} \leftarrow p_{l,t} - 1$ 
15:           $(n_1, n_2) \leftarrow (v_1, v_2)$ 
16:          break
17:        end if
18:      end if
19:    end for
20:  end for
21:   $M \leftarrow \text{AddItem}(M_a)$ 
22: end for
23: return  $M$ 

```

B. Mid-Range Plan Generation

When a team of robots is commanded to navigate an edge in the graph, we arbitrarily designate a robot to be the leader of the team and all other robots are considered followers. Each robot is then assigned a position to maintain in the formation for that edge relative to the team leader. Robots within a team share their positions and planned low-level trajectories with team members to enable predictive collision avoidance.

Based on their role in the team, we provide each robot with a mid-range plan to follow that minimizes visibility to potential observers, which we computed with A* in Section V-B8. For each robot, we continuously truncate the path to start at the closest point to the robot's current position. Additionally, we truncate the end of the leader's path to a receding horizon goal based on its maximum speed and planning time horizon. This receding horizon goal is shared with the follower robots. We then truncate each follower's path to its own receding horizon goal, which is calculated based on the leader's receding horizon goal and the follower's assigned position in the formation.

VIII. LOW-LEVEL PLANNER

After we generate a mid-level plan, it is then executed by the low-level planner, which runs decentralized on each robot.

To avoid obstacles, which may not exist in the global map, we leverage TerrainNet [40] for local mapping. TerrainNet takes RGB-D images of the environment as input and produces semantic and elevation maps as output. We produce a costmap, \mathcal{C} , by assigning a cost, $[0, 255]$, to each semantic label, which correspond to the features of the environment (e.g., bush, rock, tree, dirt, etc.) that occupy the terrain.

We represent the robots using Dubins Car kinematics with bounded wheel velocity and acceleration as follows.

$$\begin{aligned}
 \mathbf{x}_t &= [\mathbf{p}_t \ \theta_t]^T \\
 \mathbf{u}_t &= [v_t \ \alpha_t]^T \\
 \mathbf{w}_t &= \begin{bmatrix} \frac{1}{r} & \frac{b}{2r} \\ \frac{1}{r} & -\frac{r}{2r} \end{bmatrix} \mathbf{u}_t \\
 \mathbf{w}_t^{\max} &= \max(\mathbf{w}_t, \frac{v_{\min}}{r}, \mathbf{w}_{t-1} - \frac{a_{\max}}{r} \Delta t) \\
 \mathbf{w}_t^{\text{clamp}} &= \min(\mathbf{w}_t^{\max}, \frac{v_{\max}}{r}, \mathbf{w}_{t-1} + \frac{a_{\max}}{r} \Delta t) \\
 \mathbf{u}_t^{\text{clamp}} &= \begin{bmatrix} \frac{r}{2} & \frac{r}{2} \\ \frac{r}{b} & -\frac{r}{b} \end{bmatrix} \mathbf{w}_t^{\text{clamp}} \\
 \mathbf{x}_{t+1} &= \mathbf{x}_t + \begin{bmatrix} \cos(\theta_t) & 0 \\ \sin(\theta_t) & 0 \\ 0 & 1 \end{bmatrix} \mathbf{u}_t^{\text{clamp}} \Delta t
 \end{aligned} \tag{33}$$

Here \mathbf{x}_t is the state, \mathbf{p}_t is the position, θ_t is the orientation, \mathbf{u}_t is the control, v_t is the linear velocity, α_t is the angular velocity, r is the wheel radius, b is the wheel base, \mathbf{w}_t is the wheel velocities, v_{\min} is the minimum linear velocity, v_{\max} is the maximum linear velocity, a_{\max} is the maximum linear acceleration, and Δt is the discrete time step.

For local planning, we use MPPI [33]. We design our cost function to be a weighted sum of cost components to encourage: navigating towards the goal in the graph (through terms for goal distance q_d , goal heading q_h , and goal pointing

q_p), following the mid-range path (through terms for mid-range path distance q_{md} and mid-range path heading q_{mh}), and avoiding obstacle collisions, inter-robot collisions, and terrain that cannot be traversed (through terms for a costmap q_c and trajectory collision q_{tc}). Our overall cost function is as follows.

$$\begin{aligned}
 q(\mathbf{x}_t) &= \gamma_d q_d(\mathbf{x}_t) + \gamma_h q_h(\mathbf{x}_t) + \gamma_p q_p(\mathbf{x}_t) + \gamma_{md} q_{md}(\mathbf{x}_t) \\
 &\quad + \gamma_{mh} q_{mh}(\mathbf{x}_t) + q_c(\mathbf{x}_t) + q_{tc}(\mathbf{x}_t)
 \end{aligned} \tag{34}$$

In this cost function, γ_d , γ_h , γ_p , γ_{md} , and γ_{mh} are heuristically selected cost weights.

We define the difference between the current state of the robot \mathbf{x}_t and the goal state \mathbf{x}^g , the mid-range path \mathbf{x}_t^m , and the previous state \mathbf{x}_{t-1} . Additionally, we define $\Delta \mathbf{x}_{t,i}^i$, the difference between the current state of the robot and every state in the planned trajectory of each other robot on the team, $\mathbf{x}_{t,i}^i$. Here, i is the robot index and t^i is the time index along robot i 's trajectory.

$$\Delta \mathbf{x}_t^g = \mathbf{x}^g - \mathbf{x}_t \tag{35}$$

$$\Delta \mathbf{x}_t^m = \mathbf{x}_t^m - \mathbf{x}_t \tag{36}$$

$$\Delta \mathbf{x}_t = \mathbf{x}_t - \mathbf{x}_{t-1} \tag{37}$$

$$\Delta \mathbf{x}_{t,i}^i = \mathbf{x}_{t,i}^i - \mathbf{x}_t \tag{38}$$

Finally, we can define the cost components. We use parameters for goal pointing radius r_p , the maximum mid-range path cost distance d_m , the lethal costmap penalty c , the lethal costmap threshold ℓ , the trajectory collision radius r_t , and the planning time horizon T .

$$q_d(\mathbf{x}_t) = \|\Delta \mathbf{p}_t^g\| \tag{39}$$

$$\begin{aligned}
 q_h(\mathbf{x}_t) &= \exp \left(\left(\frac{\Delta \mathbf{p}_t^g}{2} \cdot \begin{bmatrix} \cos(\theta^g) \\ \sin(\theta^g) \end{bmatrix} \right)^2 \right) \\
 &\quad \cdot \min(-\cos(\Delta \theta_t^g), 0.9)
 \end{aligned} \tag{40}$$

$$\begin{aligned}
 q_p(\mathbf{x}_t) &= \mathbb{I}_{\{\|\Delta \mathbf{p}_t^g\| < r_p\}} \\
 &\quad \cdot \max(-\cos(\text{atan2}(\Delta \mathbf{p}_t^g) - \theta^g), 0)
 \end{aligned} \tag{41}$$

$$q_{md}(\mathbf{x}_t) = \min \left(\frac{\|\Delta \mathbf{p}_t^m\|}{d_m}, 1.0 \right)^2 \tag{42}$$

$$q_{mh}(\mathbf{x}_t) = \left(1 - \frac{\Delta \mathbf{p}_t}{\|\Delta \mathbf{p}_t\|} \cdot \begin{bmatrix} \cos(\theta^m) \\ \sin(\theta^m) \end{bmatrix} \right) \tag{43}$$

$$q_c(\mathbf{x}_t) = \begin{cases} 1e10, & \text{if } \mathcal{C}(\mathbf{p}_t) \geq \ell \text{ and } \mathcal{C}(\mathbf{p}_{t-1}) < \ell \\ 1e10, & \text{else if } \mathcal{C}(\mathbf{p}_t) \geq \ell \text{ and } t = T \\ c, & \text{else if } \mathcal{C}(\mathbf{p}_t) \geq \ell \text{ and } \mathcal{C}(\mathbf{p}_{t-1}) \geq \ell \\ \frac{\mathcal{C}(\mathbf{p}_t)}{\ell} & \text{otherwise} \end{cases} \tag{44}$$

$$q_{tc}(\mathbf{x}_t) = \mathbb{I}_{\{\bigvee_{i,t^i} (\|\Delta \mathbf{p}_{t,i}^i\| < r_t)\}} \cdot 1e10 \tag{45}$$

For our experiments with Clearpath Warthogs, we used the following parameters: $r = 0.279m$, $b = 1.175m$, $v_{\min} = -0.5 \frac{m}{s}$, $v_{\max} = 2.0 \frac{m}{s}$, $a_{\max} = 4.0 \frac{m}{s^2}$, $r_p = 1m$, $d_m = 10m$, $c = 30$, $\ell = 200$, $\gamma_d = 1$, $\gamma_h = 0.1$, $\gamma_p = 0.1$, $\gamma_{md} = 5.0$, and $\gamma_{mh} = 1.0$. For MPPI, we used $\Delta t = \frac{1}{15}s$, $K = 3000$ samples, time horizon $T = 5s$, temperature $\lambda = 0.01$ and sampling variance of $\Sigma = 1.94$.

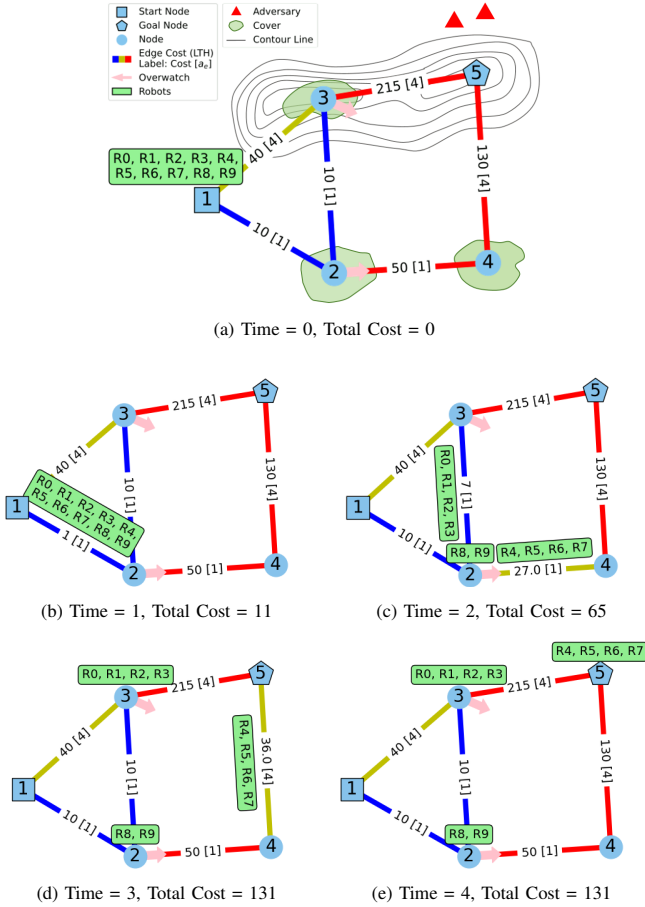


Fig. 9. MIP problem solution to an illustrative multi-robot reconnaissance scenario, sketched in (a). Ten robots start at node 1 with a goal of at least one robot reaching node 5 to observe the adversary units. The light green regions represent areas of cover. The color of the edges indicate the threat level for transitioning between nodes from low to high (LTH): blue, yellow, red. Edge (3,5) has the highest weight due to its visibility by the adversary. In each subplot, the edge labels indicate the edge cost under the current conditions and show in brackets the desired number of robots for traversal of the edge, a_e , due to vulnerability. Overwatch opportunities are shown with a pink arrow from the overwatch node pointing to the edge that can be monitored. At each time step, the position of each robot is shown.

IX. RESULTS AND DISCUSSION

We first demonstrate our graph planning approach in simulated scenarios to illustrate the advantages of our approach. We then demonstrate the full hierarchical planning architecture in hardware experiments.

A. Graph Planning Simulated Scenarios

1) *Illustrative Example:* We consider the example in Fig. 9 which depicts a simple reconnaissance scenario. There are 10 robots starting at node 1 and the goal is for at least one robot to reach node 5 while minimizing visibility. Fig. 9 steps through a solution to this problem, which we generated using our MIP optimization problem. In Fig. 9a, the edge costs are shown as the maximum cost for one robot to traverse without any overwatch, teaming, or vulnerability cost reductions. The edge labels in each subplot show the edge cost and the number of robots desired in brackets ([]). The color of the edge indicates threat level blue (lowest), yellow, or red (highest). To encourage teaming, each additional robot on an edge reduces

the cost by 1. Both directions of edges (1,3), (3,5), and (4,5) are considered vulnerable and at least four robots are desired; the cost reduction for each robot up to four is 10. Overwatch opportunities are indicated by the pink arrows. Overwatch can be provided from node 2 for both directions of edge (2,4) and node 3 for both directions of edge (4,5), which can reduce the cost by up to 20 or 60, respectively, when two robots are providing overwatch. Each additional robot providing overwatch after the first two would reduce the cost by 2. The dynamic costs incurred by each edge are updated in the graphs in Fig. 9 to reflect the teaming, vulnerability, and overwatch constructs being utilized. In this example, we scale the time cost by 10 to encourage reaching the goal in minimal time. The total accumulated cost is tracked in the captions.

In this solution, we see the robots break into three teams to work together for a subset of the robots to safely traverse to the target node. The robots all move together on edge (1,2) to get the largest benefit from teaming. Two robots then remain at node 2 to provide overwatch to the four robots traversing edge (2,4) and the remaining four continue toward node 3 to be prepared to provide overwatch in the next step. The greatest benefits from overwatch at nodes 2 and 3 are with 2 robots. Four robots (rather than two) go to node 3 to also receive a larger teaming benefit on edge (2,3) and additional rewards for overwatch in the next step. It would have been equivalent cost for two of those robots to continue on with robots 4-7. In time step 3, robots 4-7 traverse a vulnerable edge, getting the largest reward for having four robots and enabling moving in a protective formation. In the last step, robots 4-7 reach the goal node. The cost does not increase since the robots moved to a node in this step and there is no longer a time cost since there are no robots remaining on edges.

By solving our problem to optimality, we are guaranteed to have minimized the total cost. However, this depends greatly on the weights/cost assigned to the problem and the prioritization of minimizing traversing cost versus minimizing time. For example, if we did not scale our time cost by 10, the resulting solution would keep more robots together to receive more teaming benefits for moving together and from additional overwatch cost reductions. As in Fig. 9b, all robots would go to node 2. Then the robots would split into only two teams: a team for overwatch that moves from node 2 to 3 and the team being monitored on edges (2,4) and (4,5). Ultimately, requiring one additional time step.

2) *Bounding Overwatch Example:* As a demonstration of a larger graph that particularly lends itself to the bounding overwatch paradigm, Fig. 10 shows a solution to our MIP problem for the graph shown in blue. We set the start point for all robots to be node 1 and the destination for all robots is node 11. The solution yields two robot teams alternating traversing and providing overwatch. Each team's route is visualized along the edges with time steps noted to enable correlating the teams' positions and the bounding overwatch behavior.

3) *Meadow Map 1:* In Figures 11 and 12, we demonstrate applying this approach to complex real world scenarios. We consider traversing between areas of forested cover in a high-risk environment, using a simulated meadow environment from [41] as a representative example. We show results with all robots reaching a designated goal and a subset of robots

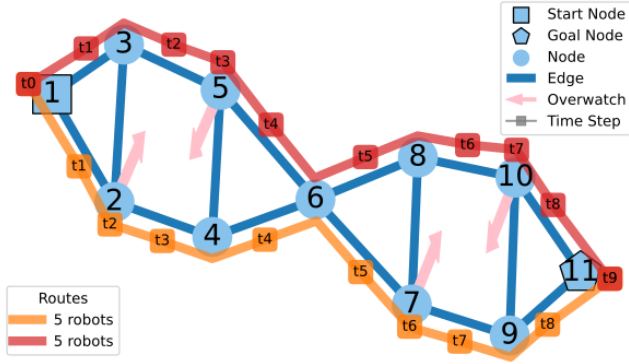


Fig. 10. Example solution demonstrating bounding overwatch behavior as all robots move from node 1 to 11. Robot team routes are shown with each time step labeled. The overwatch opportunities, indicated by the pink arrows, are met at time steps 2, 3, 6, and 7. The two teams alternate providing overwatch as they move through the environment.

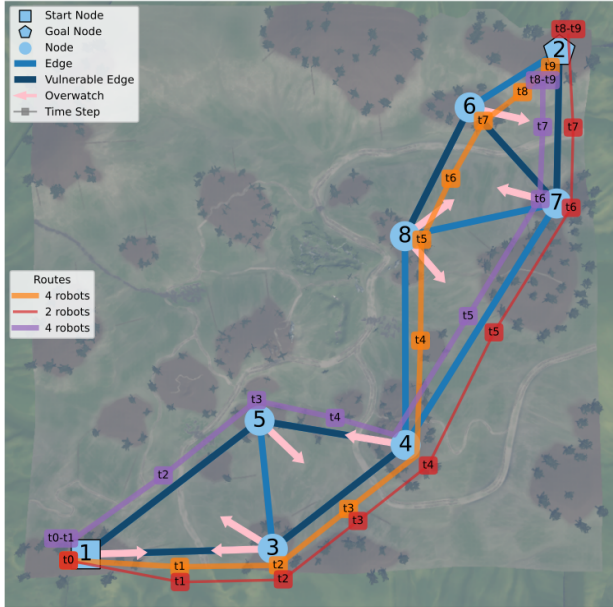


Fig. 11. Aerial map of a meadow environment showing a sample scenario. Nodes are in regions of cover. Vulnerable edges due to crossing roads are shown in dark blue. The largest teaming cost reductions on the vulnerable edges come from at least four robots traversing together. In the solution routes shown, robot teams split up and form new teams as they move through the terrain providing overwatch.

reaching the goal.

In Fig. 11, we consider 10 robots starting at node 1 with a goal of all robots reaching node 2 within 10 time steps. In our generated solution, three distinct paths emerge. Through time step 3, six robots maneuver together (orange and red teams) alternating providing overwatch with another team (purple) of four robots. At time step 4, two robots (red) remain at node 4 to provide overwatch for the purple team, while orange maneuvers toward the next overwatch position. This allows the purple and red teams to combine and proceed alternating providing overwatch with the orange team through the rest of the graph toward the goal node.

4) *Meadow Map 2*: Fig. 12 is an example with further subdivision of the robots in the solution. Again, we consider

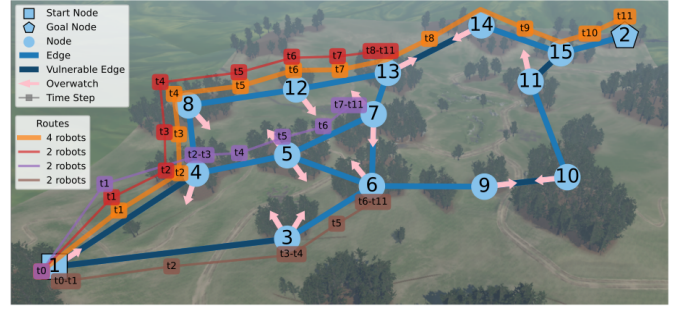


Fig. 12. Reconnaissance scenario spanning a meadow environment. The nodes are placed in forested regions of cover. Ten robots start at node 1 with the goal of at least one robot reaching node 2, across the meadow. The edges of the graph have cost for transitioning between nodes that is a function of their distance, detectability, and vulnerability. This cost can be reduced by moving in teams and by providing overwatch, where robots at a particular node oversee the movement of robots along a corresponding edge to help mitigate some of the risk of traversing. Overwatch opportunities are indicated with an arrow from the overwatch node pointing toward the edge that can be monitored. The robot team routes through the graph, solved for with our proposed method, represent a solution to this problem.

10 robots starting at node 1. In this scenario, the goal is for at least one robot to reach node 2 within 12 time steps. In this case, the solution has four teams emerge. One team of four (orange) that traverses through the map towards the goal, providing overwatch as needed, and three smaller supporting teams (red, purple, brown) providing overwatch for orange and each other. Since all robots do not need to reach the goal node, this example highlights the trade-off between the cost of traversing and the benefit of overwatch. Teams will not continue towards the goal if the overall cost of their movement is not less than the benefit of the overwatch they would provide to a primary team moving towards the goal. This concept is consistent with expectations in an operational setting: the risk outweighs the reward. Ultimately, this is the objective of our method, to be able to determine strategic tactical maneuvers in complex environments.

5) *Ablation Study*: We performed an ablation study to assess the impact of the constructs we present in Sec. III, which we label overwatch, vulnerability, and teaming, in our algorithm. Fig. 13 shows the solutions to our illustrative example when removing these components and incrementally adding them back in. The scenario is setup as in Fig. 9, with all robots starting at node 1 and an overall goal of at least one robot reaching node 5.

When we remove the overwatch, vulnerability, and teaming constructs, in Fig. 13a, the problem essentially becomes a shortest path problem. The weights in the graph are fixed and one robot takes the path with the least overall cost due to the edge weights and time. It would be an equivalent cost solution for any number of robots to take this path.

In tactical maneuvers, overwatch allows minimizing detection and maximizing safety. When we add our formulation of overwatch opportunities in Fig. 13b, the edge weights now vary based on the overwatch opportunities being utilized by the team and the optimal solution includes robots moving to the two overwatch positions while one robot traverses to the goal, overall making the operation safer.

As an incentive to travel in a formation on edges that are

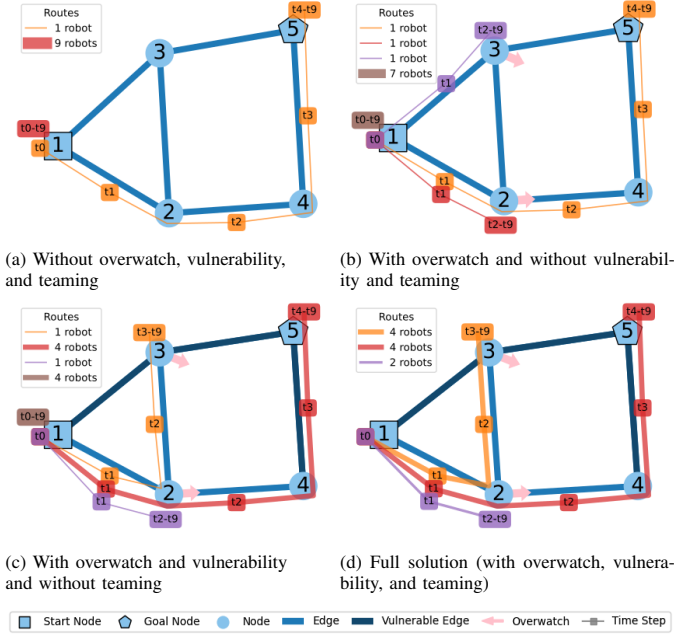


Fig. 13. Ablation study illustrating the impact of each of our main constructs: overwatch opportunities, edges with high vulnerability, and incentives for moving as a team. Robot team paths are shown in each subplot with components of our formulation incrementally added.

particularly dangerous, or vulnerable, we add our vulnerability construct back in Fig. 13c, making edges (1,3), (3,5), and (4,5) more costly to traverse alone. We see in the solution that the desired minimum of 4 robots traverse edge (4,5). The robot providing overwatch at node 3 moves with other robots on edge (1,2) and then alone on edge (2,3). This is ultimately the same cost as if four robots were to traverse the vulnerable edge (1,3). Both solutions are optimal. As in the previous cases, the extra robots stay at the start node.

In a tactical scenario, more robots moving together would provide more data, potentially reducing the overall threat level. Additionally, the redundancy of having more robots yields a more robust solution. When we add our teaming construct back into the problem, as in Fig. 13d, we see all robots moving for the first time, no longer leaving robots at the start node, since moving as a team provides cost reductions on each edge and greater cost reductions when providing overwatch. Ultimately, the overwatch, vulnerability, and teaming constructs yield practical plans for tactical maneuvers that minimize detection and maximize robustness and safe navigation.

B. Graph Planning Computation Time

The common limitation of MIP is computation time. The high level planning we propose would need to be computed rapidly (on the order of magnitude of minutes) for robots to be able to act on the plan and re-plan as new data is gathered. This allows a new plan to be generated while the robots traverse one edge of about $\sim 100 - 250m$. Table IV shows the parameters that affect the problem size for the graphs discussed in this paper (number of locations, number of overwatch opportunities, and time horizon), the total variables in our optimization problem due to those parameters, and the

TABLE IV
EXAMPLE GRAPHS' PROBLEM SIZE AND COMPUTATION TIME

	Illustr.	Bounding	Map 1	Map 2
Locations, n_L	17	43	32	51
Overwatch, n_O	4	8	18	32
Time Horizon, n_T	10	10	10	12
Total Variables	460	1160	990	1872
Mean Solve Time (s)	0.081	0.100	0.249	3.702

resulting solve time for our MIP problem in each case. The graphs are labeled Illustrative, Bounding, Map 1, and Map 2, which correspond to Figures 9 and 13, Fig. 10, Fig. 11, and Fig. 12, respectively.

We used the Gurobi optimizer [39] on an Intel® Core™ i7-10875H CPU @ 2.30GHz \times 16 and averaged the solve times across 100 trials. In all cases, the number of robots was 10. Varying the number of robots does not impact the total number of variables in our problem. We select suitable time horizons for each problem based on the size of the graph and location of the goal to ensure that the problem is feasible.

These results show computation times in seconds for realistic operational scenarios. Additionally, the problem stays computationally tractable to solve complicated routes on large graphs for multi-robot teams.

C. STALC Simulated Environment Segmentation and Graph Planning

Fig. 14 demonstrates the steps of our environment segmentation approach in a simulated meadow scenario for an observer on a hill. For a large simulated environment ($\approx 500m \times 500m$), we are able to generate a topological graph from a visibility map and we demonstrate coordinated maneuvers with a team of 3 ground vehicles. The paths of the vehicles are depicted in Fig. 14f.

D. STALC Hardware Experiments

We evaluated our hierarchical planner STALC on hardware to experimentally validate our graph generation and visibility calculations for real-world environments. Additionally, we wanted to evaluate operating with a decoupled high-level and low-level planning paradigm to ensure that the high-level plan is executable on a real-world system.

We demonstrated the ability to achieve minimum visibility planning with a team of autonomous ground vehicles with our hierarchical approach: by coupling our high-level graph-based planner with our mid-level A* planner and low-level stochastic model predictive control approach. To do this, we constructed both a visibility map and a traversability map from *a priori* data the environment.

We evaluated our approach in two highly constrained environments: forested off-road terrain and an urban environment. In both cases, the vehicles needed to avoid both static and dynamic obstacles (team members), operate in formation, and provide overwatch to their team members. We considered two different observer locations in both environments to demonstrate how the environment segmentation and ultimate route

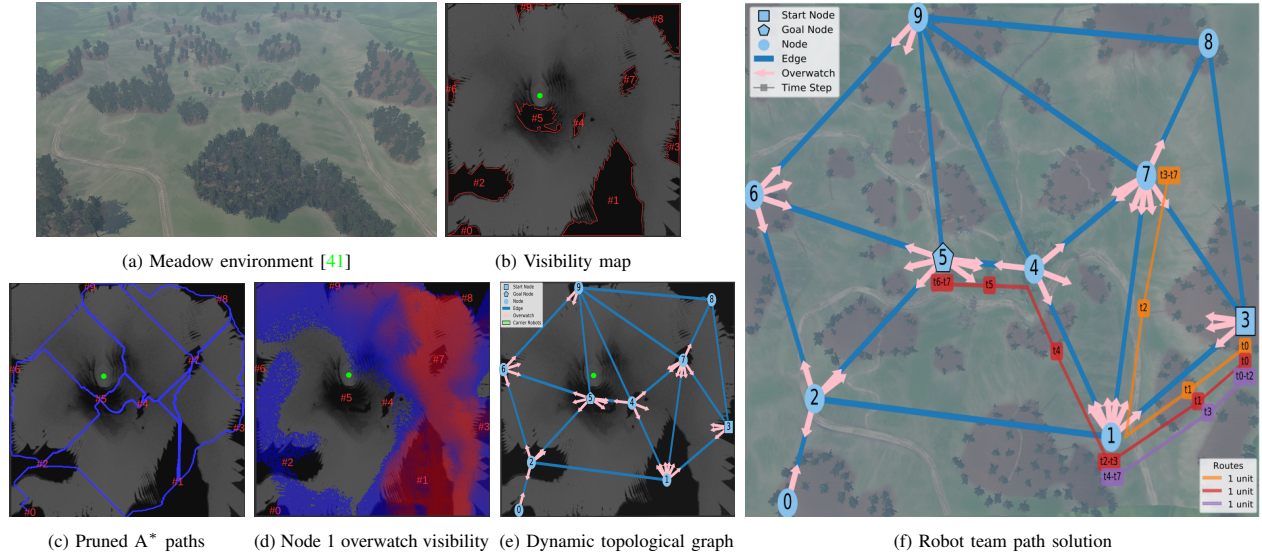


Fig. 14. Sequential steps in our environment segmentation approach for a simulated meadows environment, as seen in (a). In (b), we generate a visibility map to segment the regions of cover (outlined in red). The observer’s hilltop location is indicated by the green covariance ellipse. We then generate A* paths between these regions of cover and prune the edges between nodes based on these paths, as seen in blue in (c). For each node we generate visibility maps for oversight, (d) shows an example for node 1. Using this information, we form our topological map in (e). Overwatch opportunities are indicated from the oversight nodes to edges that can be observed with pink arrows. We then use MIP to solve for paths for each robot in the team through this graph, shown in (f). A robot team of 3 starts at node 3 with the objective of at least one robot reaching node 5 while minimizing visibility through oversight and teaming.

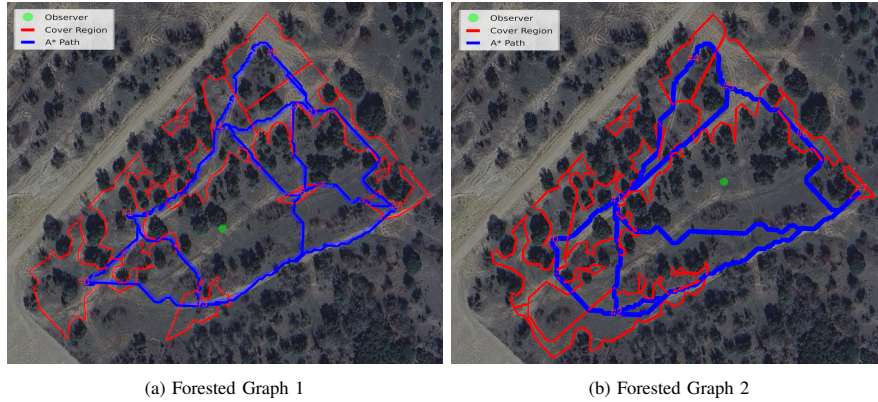


Fig. 15. Environment segmentation for two different observer locations in a forested off-road environment. Resulting cover regions and A* paths between the regions are depicted for each.

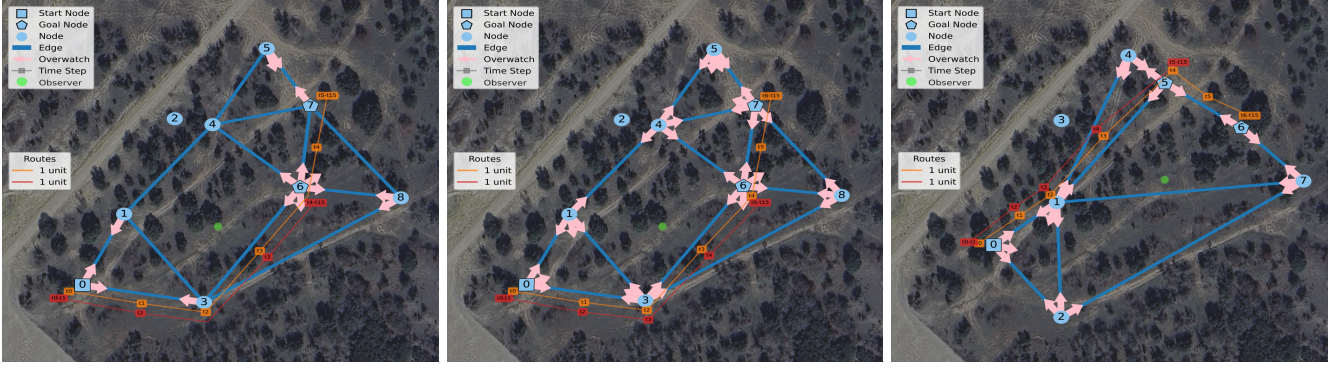
through the environment will vary based on the scenario. Additionally, we show results with different emphases on oversight versus moving in formation to demonstrate the adaptability of our graph planner to different scenario objectives.

1) *Forested Off-road Environment*: We consider a trapezoidal region of a forested off-road environment with varying types of brush, trees, and terrain. We segment the environment around two different observer locations, as depicted in Fig. 15. The change in the observer location results in significant variations in the cover regions and A* paths, ultimately resulting in different topologies for our dynamic graphs.

In Fig. 16, we illustrate a schematic representation of our topological graph with the oversight opportunities indicated. We depict the optimal team paths through the graph along the edges, as solved for using the algorithm in Table III. Between Fig. 16a and Fig. 16b, we varied the value of oversight by allowing more oversight opportunities to be considered in Fig. 16b. We do this by setting the allowable ratio of oversight

reduction to edge cost (as described in Sec. V-C) from 50% to 10%. When oversight opportunities are available, they offer a significant reduction to the edge costs and thus are desirable to be used. This results in the robots moving in formation on edge (3,6) when oversight is less valuable versus performing bounding oversight in the other case. Ultimately, in an operational scenario these types of factors and thresholds would be set based on the priorities of the scenario and the perceived risk associated with performing oversight compared to formation maneuvers (i.e., if a small amount of oversight would still be valuable to consider versus ignored in favor of moving as a team). These two different solutions on the same graph demonstrate the adaptivity of our algorithm to varying objectives.

Fig. 16b and Fig. 16c utilize the same graph planner parameters on the graphs generated from the different observer locations in Fig. 15. The observer location significantly impacts the formulation of the dynamic topological graph and



(a) Forested Graph 1 with routes prioritizing formation (b) Forested Graph 1 with routes prioritizing overwatch (c) Forested Graph 2 routes

Fig. 16. Schematic forested graphs showing overwatch opportunities and team routes for the denoted start and goal nodes. Both robots start at node 0 and the goal is for one robot to reach each goal node (nodes 6 and 7). Two different weights are used for Forested Graph 1 to show the difference in the resulting paths.

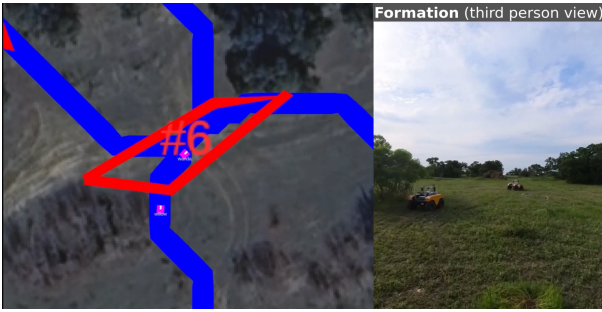


Fig. 17. Robots moving in formation approaching a cover region.



Fig. 18. Overwatch view of robot Wanda while robot Willow traverses an edge. Observer view on the top left shows the traversing robot being detectable from the observer perspective.

overwatch opportunities, ultimately resulting in significantly different routes through the environment.

Fig. 17 depicts the robots moving in formation on edge (3,6), following the paths in Fig. 16a. The vehicles maintain a set following distance along the A* paths while avoiding environmental obstacles.

Fig. 18 shows the robot Wanda performing overwatch at node 3 while the robot Willow traverses along edge (0,3). Each robot is equipped with a 360 degree camera. Additionally, the top left corner shows the observer view while Wanda is visible from the observer's perspective.

The route traversed by the robots in Forested Graph 1, in Fig. 16a and Fig. 16b, is outlined in Fig. 19. Additionally, Fig. 19 highlights the regions of this route where the robots

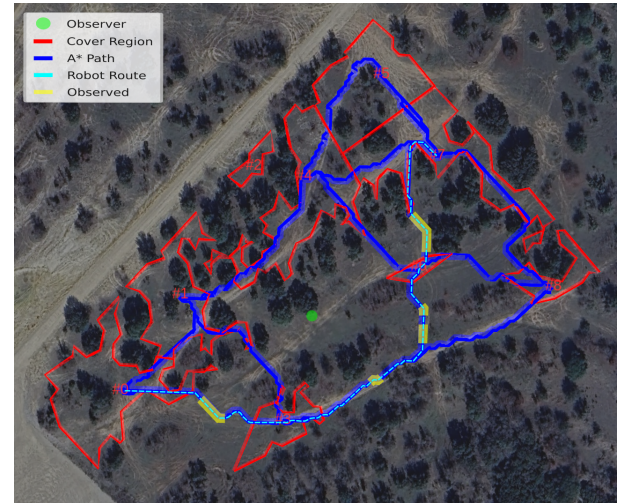


Fig. 19. Depiction of the route the robots traversed Forested Graph 1 with the regions the observer could see the robots highlighted.

were observed by a camera located at the observer position. This demonstrates that our cover regions were a conservative estimate of areas that would not be visible from the observer location.

The included video shows the robot team traversing the off-road environment using STALC following the routes in Fig. 16a.

2) *Protection Metric*: To evaluate the experimental performance of the multi-robot team, we propose the following metric to characterize the level of protection of the traversing team.

$$\mathcal{M}_{protect} = \frac{1}{n_A} \sum_{a=1}^{n_A} \frac{1}{D_a} \sum_{e \in E} (d_{o,ae} + d_{f,ae} + d_{c,ae}) \quad (46)$$

In this metric, we consider for each robot a and edge e , the distance a robot was monitored through overwatch $d_{o,ae}$, the distance traversed in formation $d_{f,ae}$, and the distance traversed in cover $d_{c,ae}$, as these are the three different forms of protection the robots can utilize for safe traversal of a region. The total distance traveled by a particular robot is D_a . We evaluate the protection metric to compare the level of

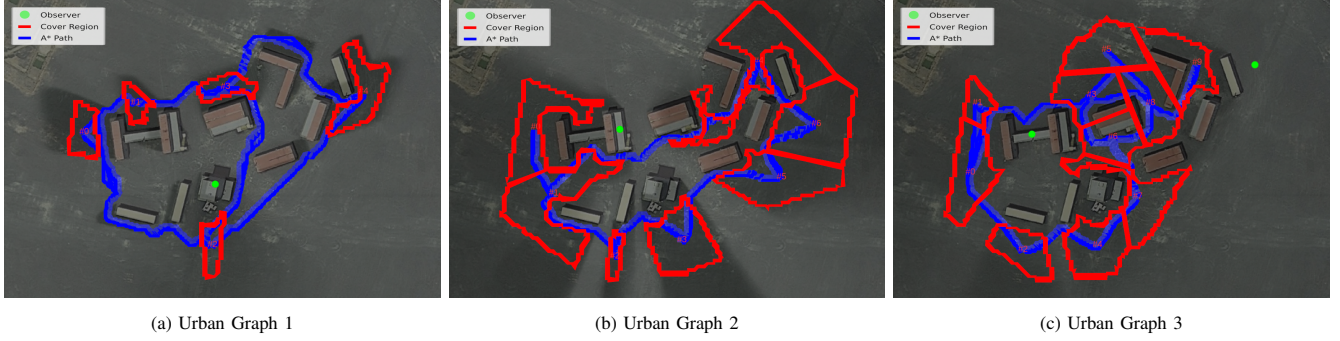
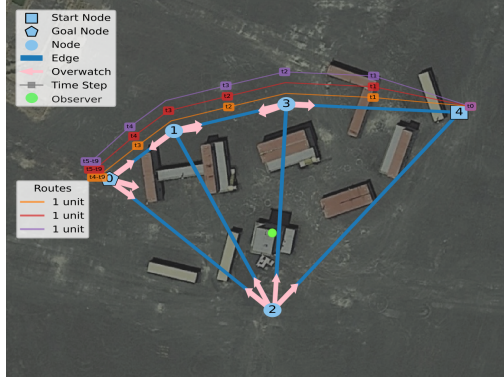


Fig. 20. Environment segmentation for three different observer locations in an urban environment, including a case with multiple observers. The visibility map is overlaid to show shadows in the regions of cover.

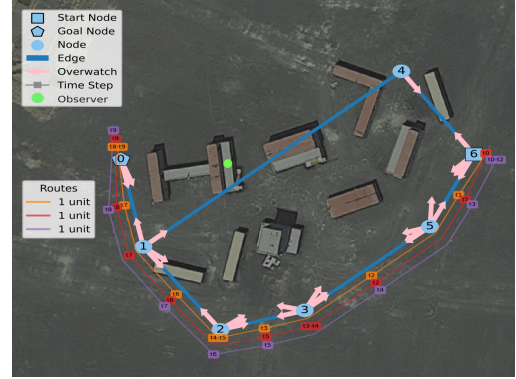


(a) Urban Graph 1 with overwatch scaled by 1

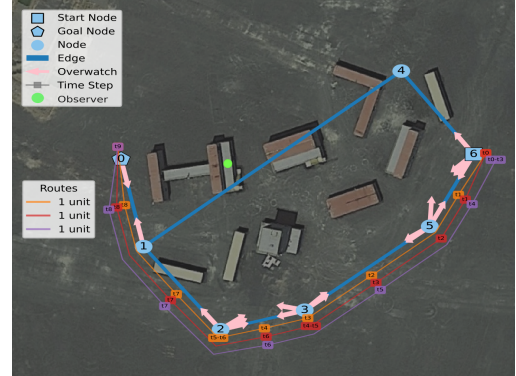


(b) Urban Graph 1 with overwatch scaled by 1.3

Fig. 21. Planned routes on Urban Graph 1 showing the difference in routes when the overwatch scale increases. In this case, this change resulted in different overwatch opportunities and a significant difference in the resulting team paths through the graph.



(a) Urban Graph 2 with overwatch scaled by 1



(b) Urban Graph 2 with overwatch scaled by 0.4

Fig. 22. Planned routes on Urban Graph 2 showing the difference in routes when the overwatch scale decreases. In this case, this change resulted in different overwatch opportunities and a subtle change to the resulting team paths through the graph.

protection between different scenarios. When a vehicle utilizes one form of protection (traversing in cover, formation, or being overwatched) throughout the entire path then this metric is $\mathcal{M}_{protect} = 1$. Additional protection will increase this score to a maximum of 3.

We consider three scenarios on Forested Graph 1 to compare the metric: two robots moving in formation on edge (3,6) following the plan in Fig. 16a, two robots moving in bounding overwatch from Fig. 16b, and a single robot traversing the route shown in Fig. 19. We present the value of the protection metric for each of these cases in Table V. As expected, the single robot scenario has the lowest score since it is not

able to be further protected by a teammate with bounding overwatch or moving in formation. In this scenario, the robots moving in formation on edge (3,6) received a higher protection metric than bounding overwatch since they can maintain visual contact with each other the entire path. In comparison, the duration of overwatch on that edge is shorter due to the brush and other terrain blocking the robot's field of view. However, the protection metric could be weighted appropriately if one form of protection is determined to be superior to the other for a particular scenario. For each of these scenarios, we computed the protection metric using camera data. A vehicle is considered to be in cover when it is not visible from the

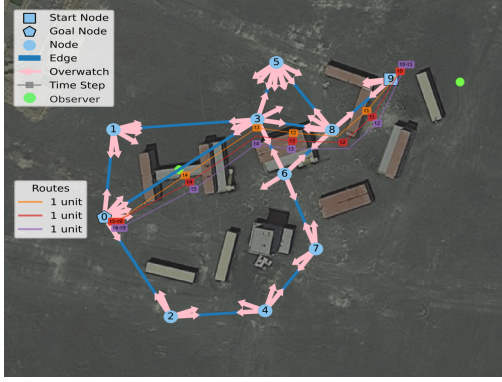


Fig. 23. Planned routes on Urban Graph 3 with two observers.

observer's location.

TABLE V
PROTECTION METRIC FOR FORESTED GRAPH 1

Scenario	Protection Metric
With Formation	1.78
Without Formation, bounding overwatch	1.65
Single Robot	0.85

3) *Urban Environment Experiments*: We considered three different segmentations of an urban environment based on different observer locations, as seen in Fig. 20. We consider two scenarios with one observer and one scenario with two observers. In Fig. 20, the visibility map for each scenario is overlaid to show shadows in the regions of cover.

We generated graph plans for the segmentations of the environment shown in Fig. 20a and Fig. 20b using two different scales for overwatch, as described in Sec. V-C. A particular scenario may consider overwatch to be more valuable and the scale factor allows that high-level guidance to vary the dynamic topological graph we consider. This demonstrates the control the user has over the high-level behaviors of the robots when generating these highly complicated paths. The resulting graph plans are shown in Fig. 21 and Fig. 22, respectively. In Fig. 23 we do not scale the overwatch (i.e., scale of 1) to instead demonstrate planning with two observer locations. From the observer regions indicated in Fig. 20, Fig. 24 shows segments of the observer's view when the robots were able to be detected in Urban Graphs 1 and 2.

Fig. 1 shows a third person view of the robots arranged at node 4 before moving into formation to traverse edge (4,3) in the first step of the plan in Fig. 21a. Fig. 1 denotes the leader and follower goal points in cover region 5 and shows the MPPI trajectories of the two robots that begin moving first. The third robot waits for the other two to get ahead of it before moving into it's position in the formation. The included video shows the STALC algorithm running in this urban environment example following the paths in Fig. 21a.

X. CONCLUSION

Our hierarchical planning approach is able to effectively generate coordinated tactics using *a priori* data while com-

pensating for changing environments with the lower-levels of the autonomy stack. We demonstrated expressing complicated scenarios compactly with a dynamic topological graph and efficient MIP formulation to yield rapid solutions to real world scenarios. We evaluated our approach in simulation and hardware experiments showing the full system operation, including swapping between overwatch and formation conditions in highly constrained environments with static and dynamic obstacles. Future research will include receding-horizon graph-based planning to update the visibility map online to account for changing conditions and a mid-range planner that utilizes the real-time sensor readings of the environment.

ACKNOWLEDGMENT

We gratefully acknowledge the support of the Army Research Laboratory under grant W911NF-22-2-0241.

REFERENCES

- [1] A. Torreño, E. Onaindia, A. Komenda, and M. Štolba, "Cooperative Multi-Agent Planning: A Survey," *ACM Computing Surveys*, vol. 50, no. 6, Nov 2017.
- [2] C. A. Dimmig, K. C. Wolfe, and J. Moore, "Multi-Robot Planning on Dynamic Topological Graphs Using Mixed- Integer Programming," in *IEEE/RSJ International Conference on Intelligent Robots and Systems (IROS)*, 2023, pp. 5394–5401.
- [3] Z. Yan, N. Jouandeau, and A. A. Cherif, "A survey and analysis of multi-robot coordination," *International Journal of Advanced Robotic Systems*, vol. 10, no. 12, p. 399, 2013.
- [4] J. K. Verma and V. Ranga, "Multi-robot coordination analysis, taxonomy, challenges and future scope," *Journal of Intelligent & Robotic Systems (JINT)*, vol. 102, pp. 1–36, 2021.
- [5] K. M. Wurm, C. Dornhege, B. Nebel, W. Burgard, and C. Stachniss, "Coordinating heterogeneous teams of robots using temporal symbolic planning," *Autonomous Robots*, vol. 34, no. 4, pp. 277–294, 2013.
- [6] M. Koes, I. Nourbakhsh, and K. Sycara, "Heterogeneous multirobot coordination with spatial and temporal constraints," in *AAAI Conference on Artificial Intelligence (AAAI)*, vol. 5, 2005, pp. 1292–1297.
- [7] B. A. Ferreira, T. Petrović, and S. Bogdan, "Distributed mission planning of complex tasks for heterogeneous multi-robot teams," *arXiv preprint arXiv:2109.10106*, 2021.
- [8] M. Limbu, Z. Hu, S. Oughourli, X. Wang, X. Xiao, and D. Shishika, "Team Coordination on Graphs with State-Dependent Edge Costs," in *IEEE/RSJ International Conference on Intelligent Robots and Systems (IROS)*, 2023, pp. 679–684.
- [9] Y. Zhou, M. Limbu, G. J. Stein, X. Wang, D. Shishika, and X. Xiao, "Team Coordination on Graphs: Problem, Analysis, and Algorithms," in *IEEE/RSJ International Conference on Intelligent Robots and Systems (IROS)*, 2024, pp. 5748–5755.
- [10] G. Sharon, R. Stern, A. Felner, and N. R. Sturtevant, "Conflict-based search for optimal multi-agent pathfinding," *Artificial Intelligence (AIJ)*, vol. 219, pp. 40–66, 2015.
- [11] M. Lagoudakis, M. Berhault, S. Koenig, P. Keskinocak, and A. Kleywegt, "Simple auctions with performance guarantees for multi-robot task allocation," in *IEEE/RSJ International Conference on Intelligent Robots and Systems (IROS)*, vol. 1, Sept 2004, pp. 698–705.
- [12] S. Park, Y. D. Zhong, and N. E. Leonard, "Multi-Robot Task Allocation Games in Dynamically Changing Environments," in *IEEE International Conference on Robotics and Automation (ICRA)*, May 2021, pp. 8678–8684.
- [13] D. Shishika and V. Kumar, "Local-game Decomposition for Multiplayer Perimeter-defense Problem," in *IEEE RAL (CDC)*, Dec 2018, pp. 2093–2100.
- [14] J. Zhou, G. Cui, S. Hu, Z. Zhang, C. Yang, Z. Liu, L. Wang, C. Li, and M. Sun, "Graph neural networks: A review of methods and applications," *AI Open*, vol. 1, pp. 57–81, 2020.
- [15] R. Kortvelesy and A. Prorok, "ModGNN: Expert Policy Approximation in Multi-Agent Systems with a Modular Graph Neural Network Architecture," in *IEEE International Conference on Robotics and Automation (ICRA)*, May 2021, pp. 9161–9167.



(a) Urban Graph 1 robots moving in formation on edge (4,3).

(b) Urban Graph 1 robot on edge (2,0).

(c) Urban Graph 2 robot on edge (5,3).

Fig. 24. Observer views for Urban Graphs 1 and 2. In (c), the tower the observer is on in Urban Graph 1 is shown on the right.

- [16] Y. Liu, W. Wang, Y. Hu, J. Hao, X. Chen, and Y. Gao, "Multi-Agent Game Abstraction via Graph Attention Neural Network," *AAAI Conference on Artificial Intelligence (AAAI)*, vol. 34, no. 05, pp. 7211–7218, Apr 2020.
- [17] L. Zhou and P. Tokekar, "Multi-robot coordination and planning in uncertain and adversarial environments," *Current Robotics Reports*, vol. 2, pp. 147–157, 2021.
- [18] M. Limbu, Z. Hu, X. Wang, D. Shishika, and X. Xiao, "Scaling team coordination on graphs with reinforcement learning," in *IEEE International Conference on Robotics and Automation (ICRA)*, 2024, pp. 16 538–16 544.
- [19] N. Mathew, S. L. Smith, and S. L. Waslander, "A graph-based approach to multi-robot rendezvous for recharging in persistent tasks," in *IEEE International Conference on Robotics and Automation (ICRA)*, May 2013, pp. 3497–3502.
- [20] N. Kamra and N. Ayanian, "A mixed integer programming model for timed deliveries in multirobot systems," in *IEEE International Conference on Automation Science and Engineering (CASE)*, Aug 2015, pp. 612–617.
- [21] M. Koes, I. Nourbakhsh, and K. Sycara, "Heterogeneous multirobot coordination with spatial and temporal constraints," in *AAAI Conference on Artificial Intelligence (AAAI)*, vol. 5, 2005, pp. 1292–1297.
- [22] E. F. Flushing, L. M. Gambardella, and G. A. Di Caro, "Simultaneous task allocation, data routing, and transmission scheduling in mobile multi-robot teams," in *IEEE/RSJ International Conference on Intelligent Robots and Systems (IROS)*, Sept 2017, pp. 1861–1868.
- [23] J. Yu and S. M. LaValle, "Optimal Multirobot Path Planning on Graphs: Complete Algorithms and Effective Heuristics," *IEEE Transactions on Robotics (T-RO)*, vol. 32, no. 5, pp. 1163–1177, Oct 2016.
- [24] B. A. Asfora, J. Banfi, and M. Campbell, "Mixed-Integer Linear Programming Models for Multi-Robot Non-Adversarial Search," *IEEE Robotics and Automation Letters (RA-L)*, vol. 5, no. 4, pp. 6805–6812, Oct 2020.
- [25] M. Hamer, L. Widmer, and R. D'Andrea, "Fast generation of collision-free trajectories for robot swarms using GPU acceleration," *IEEE Access*, vol. 7, pp. 6679–6690, 2018.
- [26] G. Wagner and H. Choset, "Subdimensional expansion for multirobot path planning," *Artificial Intelligence (AIJ)*, vol. 219, pp. 1–24, 2015.
- [27] P. Ogren and N. E. Leonard, "Obstacle avoidance in formation," in *IEEE International Conference on Robotics and Automation (ICRA)*, vol. 2, 2003, pp. 2492–2497.
- [28] X. Liang, H. Wang, Y. H. Liu, W. Chen, and T. Liu, "Formation Control of Nonholonomic Mobile Robots Without Position and Velocity Measurements," *IEEE Transactions on Robotics (T-RO)*, vol. 34, no. 2, pp. 434–446, 2018.
- [29] B. Woosley, "Efficient simultaneous task and motion planning for multiple mobile robots using task reachability graphs," Ph.D. dissertation, University of Nebraska at Omaha, 2015.
- [30] S. H. Arul, A. J. Sathyamoorthy, S. Patel, M. Otte, H. Xu, M. C. Lin, and D. Manocha, "LSwarm: Efficient collision avoidance for large swarms with coverage constraints in complex urban scenes," *IEEE Robotics and Automation Letters (RA-L)*, vol. 4, no. 4, pp. 3940–3947, 2019.
- [31] S. Kumar and S. Chakravorty, "Multi-agent generalized probabilistic RoadMaps: MAGPRM," in *IEEE/RSJ International Conference on Intelligent Robots and Systems (IROS)*, 2012, pp. 3747–3753.
- [32] P. G. Stankiewicz, S. Jenkins, G. E. Mullins, K. C. Wolfe, M. S. Johannes, and J. L. Moore, "A Motion Planning Approach for Marsupial Robotic Systems," in *IEEE/RSJ International Conference on Intelligent Robots and Systems (IROS)*, 2018, pp. 1–9.
- [33] G. Williams, P. Drews, B. Goldfain, J. M. Rehg, and E. A. Theodorou, "Aggressive driving with model predictive path integral control," in *IEEE International Conference on Robotics and Automation (ICRA)*, 2016, pp. 1433–1440.
- [34] J. Wang, G. J. Robinson, and K. White, "Generating Viewsheds without Using Sightlines," *Photogrammetric Engineering and Remote Sensing*, vol. 66, pp. 87–90, 2000.
- [35] S. Khetarpal, "Dividing A Polygon In Any Given Number Of Equal Areas," 2014. [Online]. Available: <http://www.khetarpal.org/polygon-splitting/>
- [36] R. Tyrrell Rockafellar, "Convex analysis," *Princeton mathematical series*, vol. 28, 1970.
- [37] B. Dacorogna and P. Maréchal, "The role of perspective functions in convexity, polyconvexity, rank-one convexity and separate convexity," *Journal of Convex Analysis*, vol. 15, no. 2, pp. 271–284, 2008.
- [38] T. Marcucci, J. Umenberger, P. A. Parrilo, and R. Tedrake, "Shortest Paths in Graphs of Convex Sets," *arXiv preprint arXiv:2101.11565v4*, 2022.
- [39] Gurobi Optimization, LLC, "Gurobi Optimizer Reference Manual," 2023. [Online]. Available: <https://www.gurobi.com>
- [40] X. Meng, N. Hatch, A. Lambert, A. Li, N. Wagener, M. Schmittle, J. Lee, W. Yuan, Z. Chen, S. Deng, G. Okopal, D. Fox, B. Boots, and A. Shaban, "Terrainet: Visual modeling of complex terrain for high-speed, off-road navigation," *arXiv preprint arXiv:2303.15771*, 2023.
- [41] Nature Manufacture, "Meadow - Environment Set," [Online]. Available: <https://naturemanufacture.com/meadow-environment-set/>